Alma Mater Studiorum · Università di Bologna

Scuola di Scienze
Dipartimento di Fisica e Astronomia
Corso di Laurea Magistrale in Fisica

Extended Hubbard model with soft-shoulder interaction

Relatore:
Prof. Elisa Ercolessi

Correlatori:
Prof. Fabio Ortolani
Prof. Guido Pupillo

Presentata da:
Antonello Aita

Anno Accademico 2016/2017

Un dì, s'io non andrò sempre fuggendo
di gente in gente, me vedrai seduto
su la tua pietra, o fratel mio, gemendo
il fior de' tuoi gentil anni caduto... [U. Foscolo]

A Giuseppe Forte

Abstract

Recenti studi riguardanti gli Atomi di Rydberg hanno mostrato che, tali sistemi realizzano una peculiare interazione che sembra essere attiva soltanto entro una distanza finita.
A partire da questa osservazione negli ultimi anni sono stati svolti studi teorici e sperimentali volti a descrivere le peculiari caratteristiche di tali sistemi.
Un'analisi particolarmente interessante è stata fatta focalizzando su sistemi unidimensionali implementati con bosoni hard-core e fermioni spinless, da cui è stato osservato che dal diagramma di fase si distinguono tre fasi: una prima che sembra soddisfare il paradigma dei liquidi di Luttinger, una seconda che ricalca una struttura critallina, ed una terza che si comporta come un liquido di Luttinger di cluster. Dove per cluster sono intesi particolari aggregati di particelle che vengono a formarsi in funzione del rapporto tra il raggio di interazione e la densita' di particelle nel sistema.
In questo lavoro è stato esteso lo studio a sistemi a due specie fermioniche, cercando di osservare il diagramma di fase solo in un particolare caso limite della teoria definito "limite ad una specie".
Da questa analisi si è dimostrato che in questo limite la struttura del diagramma di fase sembra ricalcare perfettamente quanto visto per i casi precedenti, in pieno accordo con le attese teoriche.

Contents

Introduction

An impressive amount of experimental and theoretical activity has characterized the recent years of ultra-cold atom physics, this can be explained by the fact that dilute, **ultra-cold gases** provide a concrete realization of many basic models of *many-body physics* [16, 17, 25].
The possibility to confine the atoms by laser light into configuration of reduced dimensionality and the perfect control and tunability of the interaction provide a novel approach for entering regimes that have never been accessible in condensed matter or nuclear physics [4].
The confinement of cold atoms in quantum wire geometry that can be achieved via strong optical lattice opens the possibility to realize both bosonic and fermionic **Luttinger liquids** [4]. An interesting class of ultra-cold atom systems are **cold-Rydberg gases** [13], that have proved to be an ideal platform to study strong interactions in many-body systems [19]. It was observed that in fermionic or hard-core boson systems in one-dimensional geometry, the interaction between the particles has a soft-core profile, so the the resulting effective potential generates a *soft-shoulder action*, it has to be intended as an interaction that acts on a finite range. This feature leads to observe that the **soft-shoulder potential** supports quantum liquid phases beyond the standard Luttinger Liquid paradigm, showing a rich phase diagram where the formation of **cluster Luttinger liquid** takes place. The breakdown of Luttinger Liquid theory has a relevant theoretical and experimental consequence as a possible emergent mechanism for strange metal phases of *cuprate high temperature superconductors* [27].
Many systems based on this interaction have been studied for the case of one species of spinless fermions and hard core bosons[10, 27].
The goal of this work consists to start to extend the analysis of these systems considering *two fermionic species*, in order to obtain a particular extension of the well know Hubbard model, that is expected to show a rich phase diagram where new phases take place.
The study of this model was performed using a very powerful numerical method the so called *Density Matrix Renormalization Group* or **DMRG** for short [34, 35].
This method was created by *Steven R. White* in 1992, he was inspired by the work about numerical renormalization group (**NRG**) of his professor *Kenneth Wilson*. Both are approximated methods that work in order to obtain the best approximation of the

ground state of systems that is impossible to treat analytically, of which is difficult to reach large size using numerically exact solutions [31].
Differently from the NRG method, that acts considering iteratively the low energy eigenstates to build the Hamiltonian of increased size of the system until it reaches the defined size, the DMRG works choosing the high weighted eigenstates of the reduced density matrix considering the system split in two subsystems [20].
The DMRG implementation can be obtained through two different algorithms, the *infinite algorithm* and the *finite algorithm*. The first works by increasing step by step the length of the system until it reachs the defined size, and the second consists to variate iteratively the subsystem size keeping fixed the system dimension the so called "sweep" [36].
Until now the DMRG is the main method to make calculations in condensed matter one dimensional systems, because it reaches spectacular accuracies such as ten decimal places in ground state energies [31]. For this work it was used a DMRG developed at the University of Bologna by the Professor *F. Ortolani* and used in many different research teams around Europe. This code works with both fermions and bosons and allows to simulate a large set of quantum systems with open and periodic boundary conditions.

The work is structured as follows: in the first chapter we will briefly introduce the *theoretical tools* used to understand the underlying models behind the studied system. We will start to explain the concept of Fermi and Luttinger liquids, and we will introduce the bosonization method and conformal field theory. In the last part of the chapter the concept of classical and quantum entropy is introduced leading us to introduce a very powerful tool of one dimensional system, the so called Calabrese-Cardy formula.
In the second chapter we will make a very detailed description of the phase diagram of the previous theoretical works concerning the soft-shoulder Hamiltonian for spinless fermions and hard-core bosons [10, 27], observing the different phases (Luttinger liquid, crystal, cluster Luttinger liquid) and the underlying phase transitions.
In the third chapter we will introduce and discuss the numerical techniques used to produce the data. Starting from exact diagonalization we will proceed to numerical renormalization group, and we will talk about DMRG technique and about the DMRG code that we utilized. In the second part of the chapter we will talk about the implementation of an exact code, made to obtain a benchmark on the input file of the DMRG code, and at the end of the chapter we will analyze some results coming from DMRG simulations on the one-species model that was first studied in [10, 27].
In the fourth chapter we will introduce the main model of the work, the so called *extended Hubbard model with soft-shoulder interaction*. We will explain the theory underlying the model and we will conclude discussing a first set of data coming from the DMRG simulation of the model.

Chapter 1

Theoretical tools

In this work we will investigate **one-dimensional models** in *quantum many body physics*.
To do this we can use a large set of theories that work very well in this sector.
We will focus on fermionic theories, observing that some times the nature of particle is not important for the description of the physics.

1.0.1 Quantum Liquids

To introduce the *one-dimensional case* let's start to talking about **interacting fermions** in the general case introducing the **Fermi liquid paradigma** [14, 24, 30].

1.0.2 Fermi Liquid

The Fermi Liquid model describes interacting fermions in high dimensional systems ($d > 1$).
We find this kind of systems at very low temperature. Contrary to the almost totality of materials they stay in the liquid phase and the quantum effects start to manifest, because of weak interaction between the particles, before they start to solidify; for example $He^4(Bose\,liquid), He^3(Fermi\,liquid)$.
To explain this behavior we have to say that "turning on" the interaction between the particles gives rise to a variation of the interpretation with respect to the *free case*. We can't describe them in terms of single particles, because their interaction influences the energetic contribution from each particle.
Instead we have to consider a new kind of particle defined as **quasi particle**.
This one is not a *real particle* but a *theoretical entity* that gives us the possibility to use mathematical tools utilized in the free case.
This point is the corner stone of the theory and it is important to give a complete description of this "new" interpretation, that consists of imagining the *quasi-particle* like

something that is made out of the whole system. This is because it is impossible to isolate a single particle, like an atom or molecule, of a strong interacting system since the latter merge together.
Only with this framework it is possible to regain definite energies and momenta and define a *dispersion relation* for the **elementary excitations** or *Landau quasi particle excitations*.
The elementary excitations are the fundamental pieces that compose the energetic spectrum, at low temperature. At these temperatures only a few such excitations are present; the excitations are long-lived and interact weakly between each other.
Let's consider these *elementary excitations* like a couple of **particle-hole** where the particle lives over the Fermi surface and the hole lives inside it.
For non interacting systems we can define the energy linked to the excitations giving the energetic difference between the particles and the holes.
For **interacting systems** we have to consider the effect of interaction that acts by influencing the distribution in *real space* and *momentum space* too, and deform the *ground state*. It follows adiabatically from some excited states of the non-interacting system.
Hence if we want to construct the interacting ground state we can try to imagine a particle with momentum **p** introduced in the system, we can consider all the particles living in a *cloud* melted together, this cloud surrounds the particle and forms something like a "*self energy cloud*". Every particle living in this condition is called "*dressed*". We can define it **quasi-particle**. In the same way it is possible to define the **quasi-hole**.
Thus the quasi-particle/hole appears as elementary excitations, and we have re-established the one-to-one correspondence between ideal and real eigenstates only for low momenta and energies, such excitations can be thought of as **sound waves**. Near the Fermi surface the concept of quasiparticle makes sense because the life time becomes sufficiently long.
The **energetic spectrum** is more complicated because of the interaction, but considering that the distribution of quasi-particles is sufficiently close to the free case we can consider the Taylor expansion of the energy:

$$E(k \sim p_F) \simeq E(p_F) + \frac{p_F}{m*}(p - p_F) \qquad v_F = \frac{p_F}{m*} \tag{1.1}$$

But most of the particle-hole excitations do not have such a linear relationship between energy and momenta; in fact, for the most part of such excitations, a given energy can correspond to many possible momenta, according with the figure (1.4).
We can see that the **momentum distribution** in the interacting case presents the same discontinuity that in the free case around k_F but differs from the step-function:

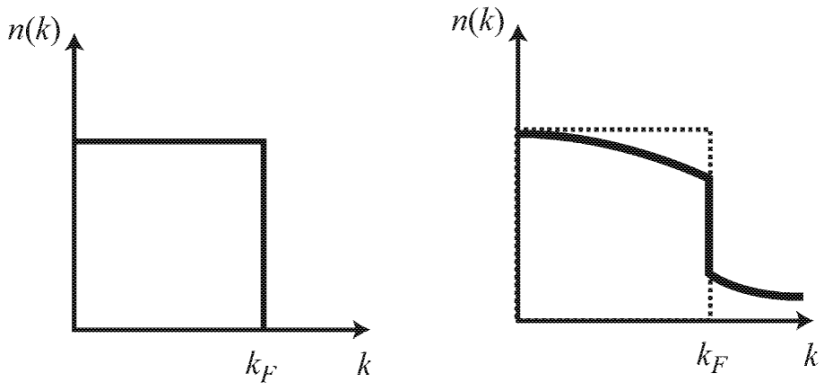

Figure 1.1: Momentum distribution in Dim > 1 (left) for free quasi-particles at T=0, (right) for interacting quasi-particles at T=0.

This discontinuity is called **quasiparticle renormalization factor** $\mathbf{z_{\tilde{k}}}$, it is equal to the *residue of the pole* in the one particle propagator. [33]

- $\mathbf{z_{\tilde{k}}} = 1$ non interacting case.
- $0 < \mathbf{z_{\tilde{k}}} < 1$ interacting case.

We can compute it from the **self-energy** $\Sigma(\vec{k}, \omega)$:

$$z_{\vec{k}} = \left(1 - \frac{\partial \Sigma}{\partial \omega}\right)^{-1}$$

This gives the discontinuity in the $n(\vec{k})$ on the Fermi surface.
Finally in a Fermi liquid the **correlation functions** decay asymptotically at long distances as a *power law* where the exponent is independent of the strength by the interaction.

1.0.3 Luttinger Liquid

In **one-dimension** the *Fermi liquid paradigma* fails. No individual motion is possible, for this reason the creation of *quasi-particle excitations* is not possible.
We find a **Collectivization** of excitations and we will assume that the ground state *breaks no symmetry*. Technically Fermi liquid theory breaks this because some vertices of the theory in one-dimension diverge because of **Peierls effect** [38].
Furthermore there is *no discontinuity* in the *momentum distribution*.

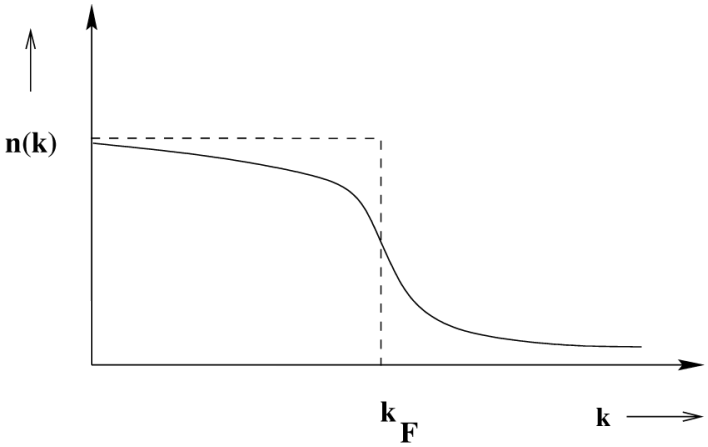

Figure 1.2: Momentum distribution in one dimension

Another important propriety is the:
Nesting of Fermi Surface that consists in the existence of a wave-vector $Q = 2k_F$ such that for a finite domain of k the energy satisfies the relation (1.2) [14].

$$\varepsilon(k+Q) = -\varepsilon(k), \qquad with \qquad \varepsilon(k) = \epsilon(k) - \epsilon_F \tag{1.2}$$

We can see that, for the aforementioned condition, a particle living below the Fermi level can jump over it, meaning above it. This because in one-dimension we find a peculiar Fermi surface as shown in figure 1.3.
The **Fermi surface** in one dimension consists of only 2 points.

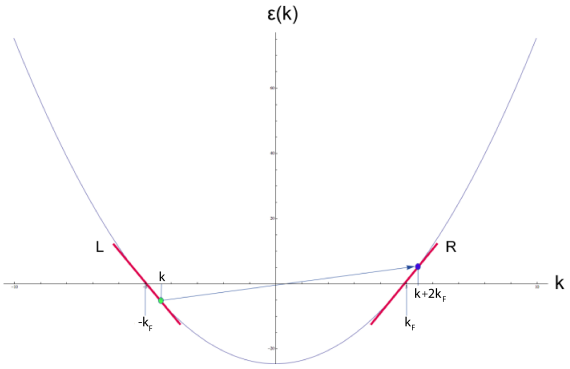

Figure 1.3: Fermi surface of free particles in one dimension

Thanks to this relation it is possible to observe the **spectrum of excitations** (1.3)

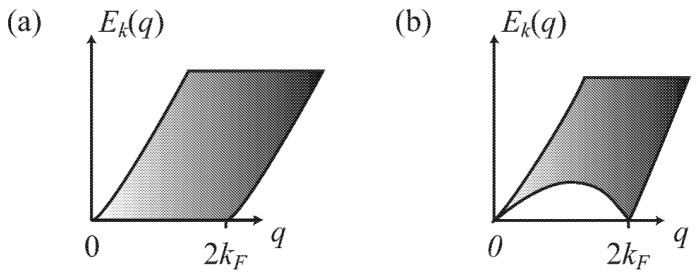

Figure 1.4: (a) Particle-hole spectrum for Dim $>$ 1, (b) Particle-hole spectrum for Dim=1.

$$E_k(q) = \varepsilon(k+q) - \varepsilon(k) \tag{1.3}$$

Given the *free spectrum* of eq (1.2) we can compute for $k \in [k_F - q, k_F]$ the average value $E(q)$ of $E_k(q)$:

$$E(q) = \frac{k_F q}{m} = v_F q \tag{1.4}$$

$$\delta E(q) = \frac{q^2}{m} \tag{1.5}$$

where $\delta E(q) = max(E_k(q)) - min(E_k(q))$, is the dispersion.
The *particle-hole excitations*, for $q \simeq 0$, are *"well defined"* particles, which become longer and longer lived when the energy tends to zero, this is possible because the life of quasi-particle is linked to the energy [14].
Finally we can say that the **correlation function** decays asymptotically at long distances as *power law*, in this case the *exponent* depends on the strength of interaction, so it means that it is not universal.
To study this phase we use two different methods:

- Bosonization
- Conformal theory

from both we can extract and define the **Luttinger Parameters**.

1.0.4 Bosonization

This is a powerful method to describe the low-energy proprieties of one dimensional systems, we will use it to obtain a formal derivation of the Luttinger liquid physics.

Free case Let's start from the simplest case, where the particles don't interact with each other.
We can re-write the Hamiltonian in second quantization, using the single particle basis:

$$H_{free} = \sum_{k,r=L,R} v_F(\epsilon_r k - k_F) {c^\dagger}_{r,k} c_{r,k} \tag{1.6}$$

we consider a **linearized spectrum** around the two Fermi points, like it is possible to see in figure 1.3.
Let us observe that we can create particle or hole excitations either around $k = -k_F$ or around $k = k_F$; we will call such excitations Right (R) and Left (L) excitations respectively.
We can see that this Hamiltonian is similar to **Dirac Hamiltonian** that describes free fermions, but this description holds only for interaction near the Fermi surface so $q \simeq 0$.
We know that a well defined energetic relation exists (1.5) for the excitations in this range, so we can try to rewrite the Hamiltonian in a different way.
The **Density Fluctuations** are thus a very natural basis to use. We can define them as superposition of *particle-hole excitations*:

$$\rho^\dagger(q) = \sum_k {c^\dagger}_{k+q} c_k \tag{1.7}$$

$$\rho(q) = \sum_k {c^\dagger}_{k-q} c_k \tag{1.8}$$

Let's see that splitting the density in terms of *right part* ($\rho_R(q) = \sum_k {c^\dagger}_{R,k+q} c_{R,k}$) and *left part* ($\rho_L(q) = \sum_k {c^\dagger}_{L,k+q} c_{L,k}$) and considering that $[{\rho^\dagger}_R(q), \rho_L(q')] = 0$, we can compute that for *periodic boundary conditions*. The commutation relations between two density fields take the form

$$[\rho_r^\dagger(q), \rho_{r'}(q')] = -\delta_{r,r'}\delta_{q,q'} \frac{rLq}{2\pi} \tag{1.9}$$

where r= L, R.
These operators act on the ground state as

$${\rho^\dagger}_R(q < 0) \left|0\right\rangle = 0 \tag{1.10}$$

$${\rho^\dagger}_L(q > 0) \left|0\right\rangle = 0 \tag{1.11}$$

then we can rewrite the operators in terms of purely bosonic operators:

$$b_r(q) = \left(\frac{2\pi}{|p|L}\right)^{\frac{1}{2}} \sum_r \Theta(rq) \rho_r(q) \tag{1.12}$$

$${b^\dagger}_r(q) = \left(\frac{2\pi}{|p|L}\right)^{\frac{1}{2}} \sum_r \Theta(rq) {\rho^\dagger}_r(q) \tag{1.13}$$

Where the Θ function is the *Heaviside step function*.
Computing the commutation relation with the Hamiltonian operator we obtain:

$$[b_r(q), H] = q v_f {b^\dagger}_r(q) \tag{1.14}$$

then we can write the Hamiltonian, in terms of these bosonic operators obtaining the next equation:

$$H \simeq \sum_{p\neq 0} v_f |p| {b^\dagger}_p b_p \tag{1.15}$$

Rather than to work directly in terms of bosons, it is convenient to switch to the use of two continuous fields:

$$\phi(x), \theta(x) = \mp(N_R \pm N_L)\frac{\pi x}{L} \mp \frac{i\pi}{L}\sum_{p\neq 0}\frac{1}{p} e^{-\alpha|p|/2 - ipx}({\rho_R}^\dagger p \pm \rho_L^\dagger(p)) \tag{1.16}$$

With some more calculations, that can be found in textbooks and reviews [14][33], we can see that the aforementioned fields satisfy the relation:

$$[\phi(x_1), \boldsymbol{\nabla}\theta(x_2)] = i\pi\delta(x_2 - x_1) \tag{1.17}$$

From the (1.17) it is possible to see that θ and $\frac{1}{\pi}\boldsymbol{\nabla}\phi(x)$ are canonically conjugate.
Hamiltonian (1.15) can be rewritten in terms of the continuum fields (1.16) [14] as follows

$$H_{free} = \frac{1}{2\pi}\int \mathrm{d}x\, v_f \left[(\pi\boldsymbol{\nabla}\theta(x))^2 + (\boldsymbol{\nabla}\phi(x))^2\right] \tag{1.18}$$

Interacting case We can introduce an interaction in this model which is quadratic in the fermion density

$$H_{int} = \alpha \sum_{k,k',p} V(q) {c^\dagger}_{k+q} {c^\dagger}_{k'-q} c_{k'} c_k \tag{1.19}$$

The fact that in one dimension the *Fermi surface* is reduced to two points allows us to decompose the interaction in three different sectors, we will consider only the first two, because the third is not realizable for only one species (like spinless fermion). These two are shown in figure 1.5.

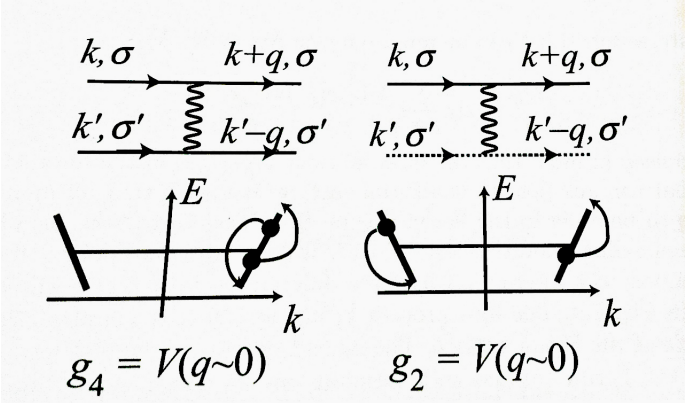

Figure 1.5: Low energy process of interaction.
A full line is for a fermion with a momentum close to $+k_F$ and dashed line for a fermion with momentum close to $-k_F$.
Figure extracted from [14]

.

With the notation "g" we designate the so-called *g-ology*.
We can compute the "g" analytically working with the **Feynman diagram** shown in figure 1.5. To do it we can use the *Dzyaloshinskii-Larkin solution* [14] that is an exact solution of the model just for the spinless case or the **renormalization group** that is a very powerful analytical method [14].
We can now rewrite the Hamiltonian in terms of *density fluctuations*

$$H_{int} = \sum_{\substack{q>0 \\ r,r'=L,R}} \beta_{r,r'} {\rho^\dagger}_r(q)\rho_{r'}(q) \tag{1.20}$$

where the elements of matrix are $\beta_{R,R} = g_4$, $\beta_{R,L} = g_2$.
We can rewrite the *density (left/right) operator* using Fourier transforms:

$$\rho_\sigma(x) = \frac{1}{\Omega}\sum_{k,q} e^{-iqx} {c^\dagger}_{k+q,\sigma} c_{k,\sigma} \tag{1.21}$$

We can rewrite the Hamiltonian in terms of the (1.21), and obtaining the Hamiltonian as follows

$$\begin{aligned} H_{int} = \frac{g_4}{2}\int_0^L \mathrm{d}x\, \rho_R(x)\rho_R(x) + \frac{g_2}{2}\int_0^L \mathrm{d}x\, \rho_R(x)\rho_L(x) + \\ + \frac{g_4}{2}\int_0^L \mathrm{d}x\, \rho_L(x)\rho_L(x) + \frac{g_2}{2}\int_0^L \mathrm{d}x\, \rho_L(x)\rho_R(x) \end{aligned} \tag{1.22}$$

Considering the transformations between the density fluctuations and the two previous fields $\phi(x)\,,\,\theta(x)$

$$\boldsymbol{\nabla}\phi(x) = -\pi[\rho_R(x) + \rho_L(x)] \tag{1.23}$$
$$\boldsymbol{\nabla}\theta(x) = \pi[\rho_R(x) - \rho_L(x)] \tag{1.24}$$

we can rewrite the Hamiltonian for the interacting part as

$$H_{int} = \frac{1}{2\pi}\int_0^L \mathrm{d}x\ \left\{(\boldsymbol{\nabla}\phi(x))^2\left[\frac{g_4}{4\pi} + \frac{g_2}{4\pi}\right] + (\boldsymbol{\nabla}\theta(x))^2\left[\frac{g_4}{4\pi} - \frac{g_2}{4\pi}\right]\right\} \tag{1.25}$$

Let's merge the equations (1.18) and (1.25) to obtain a more compact Hamiltonian

$$H = \frac{1}{2\pi}\int_0^L \mathrm{d}x\ \left\{uK(\boldsymbol{\nabla}\phi(x))^2 + \frac{u}{K}(\boldsymbol{\nabla}\theta(x))^2\right\} \tag{1.26}$$

$$uK = \left[1 + \frac{g_4}{4\pi v_F} + \frac{g_2}{4\pi v_F}\right] v_f \tag{1.27}$$
$$\frac{u}{K} = \left[1 + \frac{g_4}{4\pi v_F} - \frac{g_2}{4\pi v_F}\right] \tag{1.28}$$

We can see that the Hamiltonian remains *quadratic* even in the presence of interactions. The latter are absorbed in two parameters:

- **u** renormalized velocity
- **K** Luttinger Parameter

Depending on their value we can find the class of universality to which it belongs.

Correlation function Considering the case of continuum *fermionic field operator*

$$\psi(x) = \frac{1}{\sqrt{\Omega}}\sum_k e^{ikx}c_k \tag{1.29}$$
$$\psi^\dagger(x) = \frac{1}{\sqrt{\Omega}}\sum_k e^{-ikx}c^\dagger{}_k \tag{1.30}$$

It is possible to split each operator into two different kinds of operators

$$\psi(x) = \psi_R(x) + \psi_L(x) \tag{1.31}$$

Then we consider the **density operator** in real coordinates

$$\rho(x) = \psi^\dagger(x)\psi(x) = \psi_R^\dagger(x)\psi_R(x) + \psi_L^\dagger(x)\psi_L(x) + [\psi_R^\dagger(x)\psi_L(x) + h.c.] \tag{1.32}$$

We can rewrite the density operator using the relations (1.32) [14] obtaining:

$$\rho(x) = -\frac{\boldsymbol{\nabla}\phi(x)}{\pi} + \frac{1}{2\pi\alpha}\left[e^{i(k_F x - \phi(x))} + h.c.\right] \tag{1.33}$$

The **density-density** correlation, at equal times , thus becomes in real space:

$$< \rho(x)\rho(0) >= \frac{1}{\pi^2} < \boldsymbol{\nabla}\phi(x)\boldsymbol{\nabla}\phi(0) > + \frac{1}{2\pi\alpha}[e^{i2k_F x} < e^{i<2\phi(x) - 2\phi(0)>} > + h.c.] \tag{1.34}$$

Applying some algebra, as explained in [14], we can re-write the (1.34) as follows

$$< \rho(x)\rho(0) >= \frac{K}{2\pi^2}\frac{{y^2}_\alpha - x^2}{({y^2}_\alpha + x^2)^2} + \frac{2}{(2\pi\alpha)^2} cos(2k_F x)\left(\frac{\alpha}{x}\right)^{2K} \tag{1.35}$$

Where K is the aforementioned *Luttinger parameter*, α is a non universal constant, y_α is the renormalized interaction.

Phenomenological bosonization

To define a link between the previous observables and the quantity that we can observe from the simulation we can introduce a more general way to express the previous results. We can define the *density operator*

$$\rho(x) = \sum_i \delta(x - x_i) \tag{1.36}$$

where x_i is the position of each particle that we can define as:

$$x_i = R_i + u_i \tag{1.37}$$

where $R_i = di$ is the *equilibrium position* given by the *average distance* $d = 1/\rho_0$ (ρ_0 is the average density), "i" is the integer number that labels the particle and u_i is the displacement relative to the equilibrium position.
Let's choose a labelling field $\phi_l(x)$ that is a continuous function of the position, we show a representation of this in figure 1.6.

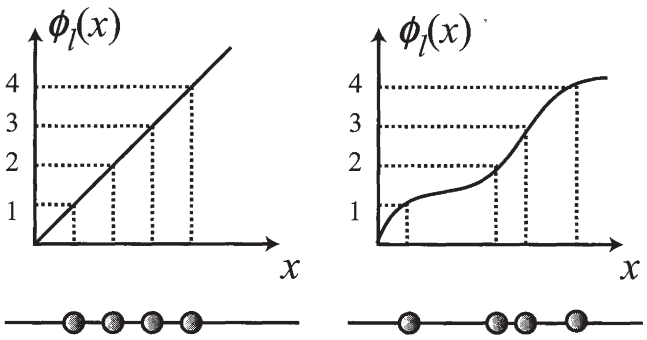

Figure 1.6: Some examples of the labeling field $\phi_l(x)$.
Figure extracted from the reference book [14].

This field behaves like a straight line when the particles form a perfect order of lattice spacing d, and starts to oscillate around the line when the particles live at any other position.
Using this labeling field and the rule for transforming the δ function, we can rewrite the density operator:

$$\rho(x) = \sum_i \delta(x - x_i) = \sum_i |\boldsymbol{\nabla}\phi_l(x)|\delta(\phi_l(x) - 2\pi i) \tag{1.38}$$

Using the *Poisson summation formula* [14] we can rewrite

$$\rho(x) = \frac{\boldsymbol{\nabla}\phi_l(x)}{2\pi} \sum_p e^{ip\phi_l(x)} \tag{1.39}$$

We can rewrite the labeling field in terms of a convenient field relative to the perfect crystalline solution, as is it shown in the next formula:

$$\phi_l(x) = 2\pi\rho_0 x - 2\phi(x) \tag{1.40}$$

so the density becomes

$$\rho(x) = \left[\rho_0 - \frac{1}{\pi}\boldsymbol{\nabla}\phi(x)\right] \sum_p e^{i2p(\pi\rho_0 x - \phi(x))} \tag{1.41}$$

Let's define the *single particle creation operator*

$$\psi^\dagger(x) = \sqrt{\rho(x)}e^{-i\theta(x)} \tag{1.42}$$

where $\theta(x)$ is some operator.
Considering that these particles are *bosons*, they have to satisfy the commutation relation

$$[\psi_B(x), \psi_B(x')] = \delta(x - x') \tag{1.43}$$

A sufficient condition to satisfy the (1.43) would be

$$[\rho(x), e^{-i\theta(x')}] = \delta(x - x')e^{-i\theta(x')} \tag{1.44}$$

If we consider the density written like in formula (1.39) the (1.45) is obviously satisfied

$$[\frac{1}{\pi}\boldsymbol{\nabla}\phi(x), \theta(x')] = -i\delta(x - x') \tag{1.45}$$

The last result (1.45) gives a proof that θ and $\boldsymbol{\nabla}\phi$ are *canonical conjugate*.
If we want to write the Hamiltonian describing the low energy proprieties of a *massless one-dimensional system* in terms of the variables $\phi(x)$ and $\theta(x)$, we have to consider that the terms $(\boldsymbol{\nabla}\theta(x))^2$ and $(\boldsymbol{\nabla}\phi(x))^2$ have to be present, so we can write

$$H = \frac{1}{2\pi}\int \mathrm{d}x \ \left\{uK(\boldsymbol{\nabla}\phi(x))^2 + \frac{u}{K}(\boldsymbol{\nabla}\theta(x))^2\right\} \tag{1.46}$$

that is the same to (1.26).
We can see that the density-density correlation functions are practically written in the same way as the previous one (1.35)

$$< \rho(x)\rho(0) >= \rho_0^2 + \frac{K}{2\pi^2}\frac{{y^2}_\alpha - x^2}{({y^2}_\alpha + x^2)^2} + \frac{A_2\rho_0}{(2\pi\alpha)^2}cos(2\rho_0 x)\left(\frac{\alpha}{x}\right)^{2K} + \dots \tag{1.47}$$

From this one it is possible to consider just the connected part, obtaining the next equation

$$G_2(x) = \frac{K}{2\pi^2}\frac{{y^2}_\alpha - x^2}{({y^2}_\alpha + x^2)^2} + \frac{A_2\rho_0}{(2\pi\alpha)^2}cos(2\rho_0 x)\left(\frac{\alpha}{x}\right)^{2K} + \dots \tag{1.48}$$

We can say that the first part of the previous equation is linked to the conformal behavior and the second part is linked to the spatial distribution of the particle in the lattice.
In reality it is more comfortable to work with the Fourier transform of the *connected density-density correlation* which is named **Structure factor**. We can write it for the finite lattice:

$$S(k) = \sum_{j,l=1}^{L} e^{ik(j-l)}\frac{G_2(j-l)}{L} \tag{1.49}$$

Where l, j are the labels of the sites. From the structure factor it is possible to extract the Luttinger parameter (K) expanding around the $k \sim 0$.

1.0.5 Conformal Theory

What found in the previous section shows that the correlation of a Luttinger liquid corresponds to the correlation of a classical two-dimensional system that sits exactly at

critically [14].
In this condition the propriety of the system at the critical point is described by a *Field Theory*.
At the **crytical point** the correlation length goes to infinity, so the field theory becomes **massless** and **scale invariant** under transformation of the coordinates.

$$x_a \to \lambda x_a \tag{1.50}$$
$$\phi_i \to \lambda_i^d \phi_i \tag{1.51}$$

where d is an *anomalus dimension*, an important value that influences all the *critical exponents* [28].
These invariances are simply a consequence of the irrelevance of the detailed lattice structure for critical behavior.
By requiring the covariance under *translation, rotation and scale invariance*, we can see that the **energy-momentum tensor** is *symmetric* and *traceless*, this result is called in literature **Poliakov Theorem** [28].

Since this already implies the covariance of scaling operators under **conformal transformation**, we can say that, rather than being an extra requirement, conformal field invariance is the logical extention of scale invariance [18].

Conformal theory $D > 2$

When we require a conformal transformation of the coordinates, the metric has to transform in this way:

$$g'_{\mu\nu}(x') = \Lambda(x) g_{\mu\nu}(x) \tag{1.52}$$

we can give the infinitesimal form of these transformations:

$$x^\mu \to x'^\mu = x^\mu + \epsilon^\mu(x) \tag{1.53}$$

If we want to preserve the conservation of the *line element* (1.54)

$$ds^2 = g_{\mu\nu} dx^\mu dx^\nu \tag{1.54}$$

the metric has to transform like shown in the next formula:

$$g'_{\mu\nu}(x') = \frac{\partial x^\alpha}{\partial x'^\mu} \frac{\partial x^\beta}{\partial x'^\nu} g'_{\mu\nu} \tag{1.55}$$

Expanding the transformations (1.55) the metric becomes:

$$g'_{\mu\nu}(x') = g_{\mu\nu}(x) + (\partial_\mu \epsilon_\nu(x) + \partial_\nu \epsilon_\mu(x)) \tag{1.56}$$

Requiring the invariance of the metric the transformations (1.56) have to satisfy the relation (1.57).

$$\partial_\mu \epsilon_\nu(x) + \partial_\nu \epsilon_\mu(x) = \rho(x) g_{\mu\nu} \tag{1.57}$$

The form of ρ can be calculated computing the trace of both the parts of the equation (1.57)

$$\rho(x) = \frac{2}{D} \partial \cdot \epsilon \tag{1.58}$$

where D is the dimension of the space where we are working.
Substituting the (1.58) inside the (1.58) and considering that the conformal transformations are an infinitesimal deformation of the standard Cartesian metric ($g_{\mu,\nu} = \delta_{\mu,\nu}$) we obtain

$$\partial_\mu \epsilon_\nu(x) + \partial_\nu \epsilon_\mu(x) = \frac{2}{D} \partial \cdot \epsilon \delta_{\mu\nu} \tag{1.59}$$

let's rewrite it in a different way

$$[\delta_{\mu\nu} \Box + (D-2) \partial_\mu \partial_\nu] \partial \cdot \epsilon = 0 \tag{1.60}$$

The ϵ's are the generators of the conformal group in $D > 2$, whose representations are finite dimensional. In particular one has:

$$(translation) \quad \epsilon^\mu = a^\mu \qquad x'^\mu = x^\mu + a^\mu \tag{1.61}$$

$$(dilation) \quad \epsilon^\mu = \lambda x^\mu \qquad x'^\mu = \alpha x^\mu \tag{1.62}$$

$$(rigid\, rotation) \quad \epsilon^\mu = \omega^{\mu\nu} x^\nu \qquad x'^\mu = M^\mu - \nu x^\nu \tag{1.63}$$

$$(SCT) \quad \epsilon^\mu = b^\mu x^2 - 2 x^\mu b \cdot \qquad x'^\mu = \frac{x^\mu - b^\mu x^2}{1 - 2b \cdot x + b^2 x^2} \tag{1.64}$$

Where (SCT) means *Special Conformal Transformations*.
We can see that in the Euclidean D-dimensional space there is a finite number of generators, as it is possible to see in the textbook [12].
The generators of this symmetry yields the group $SO(D+1,1)$ which has a number of generators given by:

$$\frac{(D+1)D + 2}{2} \tag{1.65}$$

Conformal theory D=2

Conformal field theories describe the macroscopic fluctuations in two-dimensional critical phenomena based on the representation theory of underlying infinite dimensional systems [15]. Let's observe that the equation (1.59) in the case of D=2 gives

$$\partial_1 \epsilon_1 = \partial_2 \epsilon_2 \qquad \partial_2 \epsilon_1 = -\partial_1 \epsilon_2 \tag{1.66}$$

$$\partial_2 \epsilon_1 = \partial_1 \epsilon_2 \qquad \partial_1 \epsilon_1 = -\partial_2 \epsilon_2 \tag{1.67}$$

We can see that these are the **Chauchy-Riemann equations**, it means that the generators of the symmetry have to be **Holomorphic functions** that in this case are equivalent to *analytic functions*.
We can see that the (1.66) represents the *Holomorphic part* and the (1.67) the *Anti-Holomorphic part*, for simplicity we will write all the calculations for the Holomorphic case but the they are practically the same for the other part.
By remembering the holomorfic propriety, we can express the infinitesimal transformation as

$$z' = z + \epsilon(z) \qquad z \in \mathbb{C} \tag{1.68}$$

$$\epsilon(z) = \sum_{-\infty}^{\infty} c_n z^{n+1} \tag{1.69}$$

where by hypothesis, the infinitesimal mapping admits a **Laurent expansion** around $z = 0$, the effect of such a mapping on a spinless and dimensionless field $\phi(z, \bar{z})$ living on the plane is

$$\phi'(z', \bar{z'}) = \phi(z, \bar{z}) + \delta\phi(z, \bar{z}) \tag{1.70}$$

$$\begin{aligned} \delta\phi(z, \bar{z}) &= -\epsilon(z)\partial\phi(z, \bar{z}) - \bar{\epsilon}(\bar{z})\bar{\partial}\phi(z, \bar{z}) = \\ &= \sum_n \{c_n l_n \phi(z, \bar{z}) + \bar{c}_n \bar{l}_n \phi(z, \bar{z})\} \end{aligned} \tag{1.71}$$

where we have introduced the generators

$$l_n = -z^{n+1}\partial_z \qquad \bar{l}_n = -\bar{z}^{n+1}\partial_{\bar{z}} \tag{1.72}$$

These operators obey to the following commutation relations

$$\begin{aligned} [l_n, l_m] &= (n - m)\delta_{m,n} \\ [\bar{l}_n, \bar{l}_m] &= (n - m)\delta_{n,m} \\ [l_n, \bar{l}_m] &= 0 \end{aligned} \tag{1.73}$$

this is called *Witt algebra* and it is an infinite algebra.
It seems that the situation is quite different in two dimensions, but we can see that each of these two infinite-dimensional algebras contains a *finite sub-algebra* (l_{-1}, l_0, l_1) this one is linked to the *global conformal transformation*.
We can see that the elements of this sub algebra are linked to the following transformations:

$$l_{-1} = -\partial_z \qquad translation \tag{1.74}$$

$$l_0 = -z\partial_z \qquad scale\, and\, rotation \tag{1.75}$$

$$l_1 = -z^2\partial_z \qquad special\ conformal\ tranformation \tag{1.76}$$

A complete set of global conformal transformations is given by the **Moebius transformations** or **projective transformation** that we can write:

$$f(z) = \frac{az+b}{cz+d} \qquad with \quad ad-bc = 1\,,\; a,b,c,d \in \mathbb{C} \tag{1.77}$$

they depend on four complex parameters, but one of them is fixed by the constraint so only three complex parameters are free.
Three complex parameters are equivalent to six real parameters, like required by the general theory.
Let's introduce the concept of **primary field**, defined as a field whose variation under any local conformal transformation in two dimensions is of the form:

$$z' \to z' = f(z)$$

$$\phi'(z',\bar{z}') = \left(\frac{\partial z'}{\partial z}\right)^{-h}\left(\frac{\partial \bar{z}'}{\partial \bar{z}}\right)^{-\bar{h}}\phi(z,\bar{z}) \tag{1.78}$$

where the $(h,\bar{h})$ are named **conformal dimensions** [12, 15] .
These two values are very important because we can see that they define the esponential decay of the **Correlation functions**

$$< \phi_1(z_1,\bar{z}_1),\phi_2(z_2,\bar{z}_1) >= \frac{C_{12}}{(z_1-z_2)^{2h}(\bar{z}_1+\bar{z}_2)^{2\bar{h}}} \tag{1.79}$$

where $h_1 = h_2 = h$ and $\bar{h}_1 = \bar{h}_2 = \bar{h}$ if ϕ_1, ϕ_2 are the same field.
To observe a particular feature that characterizes every theory we look at the transformation of energy-momentum tensor:

$$\delta_\epsilon\langle T(w)\rangle = -\frac{1}{2\pi i}\oint_C \mathrm{d}z\,\epsilon(z)T(z)T(w)$$

$$= -\frac{1}{12}c\partial_w^3\epsilon(w) - 2T(w)\partial_w\epsilon(w) - \epsilon(w)\partial_w T(w) \tag{1.80}$$

where

$$z \to w(z) = z + \epsilon(z)$$

We can rewrite the stress-energy tensor as

$$T'(w) = \left(\frac{\mathrm{d}w}{\mathrm{d}z}\right)^{-2}\left[T(z) - \frac{c}{12}\{w;z\}\right] \tag{1.81}$$

the last term of the previous equation is named *Schwarzian derivative*, and it is what makes different the stress-energy tensor from a primary field. Indeed it is said to be a secondary field.
The "c" that appears in the previous term is named **Central Charge**, also known as *conformal anomaly*.

Operator formalism

Here we try to rewrite the Hamiltonian in a different way, in terms of particular operators. In fact we can define

$$Q_\epsilon = \delta_\epsilon \langle T(w) \rangle \tag{1.82}$$

which helps us to compute the infinitesimal transformation of a primary field, in order to show directly the generators of the transformation

$$\delta_\epsilon \phi(w) = -[Q_\epsilon, \phi(w)] = iG_\epsilon \phi(w) \tag{1.83}$$

To obtain it we can rewrite the conformal charge in terms of the operators of the conformal-infinite algebra (1.74)

$$\begin{aligned} Q_\epsilon &= \frac{1}{2\pi i} \oint \mathrm{d}z \left(\sum_{n\in\mathbb{Z}} z^{n+1} \epsilon_n \right) T(z) = \\ &= \sum_{n\in\mathbb{Z}} \epsilon_n \oint \frac{\mathrm{d}z}{2\pi i}\, z^{n+1} T(z) = \\ &= \sum_{n\in\mathbb{Z}} \epsilon_n L_n \end{aligned} \tag{1.84}$$

So we can express the energy-momentum tensor in terms of these new operators

$$T(z) = \sum_{n\in\mathbb{Z}} z^{-n-1} L_n \qquad , \qquad L_n = \frac{1}{2\pi i} \oint \mathrm{d}z\, z^{n+1} T(z) \tag{1.85}$$

These operators satisfy another algebra named **Virasoro Algebra**

$$\begin{aligned} [L_n, L_m] &= (n-m) L_{m+n} + \frac{c}{12} n(n^2-1)\delta_{n+m,0} \\ [\bar{L}_n, \bar{L}_m] &= (n-m) L_{m+n} + \frac{c}{12} n(n^2-1)\delta_{n+m,0} \\ [L_n, \bar{L}_m] &= 0 \end{aligned} \tag{1.86}$$

Let's build the **Hilbert space** of a conformal field theory.
We will start from the *vacuum state* that has to be invariant under global conformal transformations, this can be recovered from condition

$$T(z)\,|0\rangle = \bar{T(z)}\,|0\rangle = 0 \tag{1.87}$$

$$L_n\,|0\rangle = \bar{L_n}\,|0\rangle \qquad (n \geq -1) \tag{1.88}$$

We can show the commutation relation between the primary field and the L_n operator of Virasoro algebra are given by

$$[L_n, \phi(w,\bar{w})] = h(n+1)\bar{w}^n \phi(w,\bar{w}) + w^{n+1}\partial\phi(w,\bar{w}) \tag{1.89}$$

and similarly for the operators $\bar{L}_n$.
We can define the state $|h, \bar{h}\rangle$ as the primary field calculated at the origin, acting on the vacuum state:

$$|h, \bar{h}\rangle = \phi(0,0)\,|0\rangle \tag{1.90}$$

using (1.89) we obtain:

$$L_0\,|h, \bar{h}\rangle = h\,|h, \bar{h}\rangle \qquad \bar{L}_0\,|h, \bar{h}\rangle = \bar{h}\,|h, \bar{h}\rangle \tag{1.91}$$

Representation of conformal theory on cylinder

Depending on the features of the system that we will analyze, we will consider a particular representation that takes into account periodic boundary conditions.
Let's consider the cylindric space

$$\sigma_0 \in (-\infty, \infty)\,, \quad \sigma_1 \in [0, 2\pi]\,, \quad z \in \mathbb{C}$$

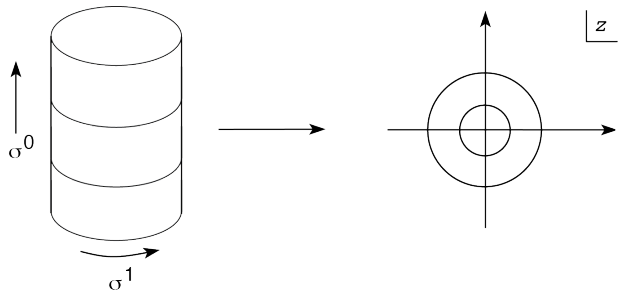

Figure 1.7: figure extracted by [15]

It exists a *conformal map* that links these two spaces

$$\eta = \sigma_0 + i\sigma_0 = \frac{L}{2\pi} ln(z) \tag{1.92}$$

Substituting the (1.92) into (1.81) [22] we find

$$H = \frac{2\pi}{L}(L_0 - \bar{L_0}) - \frac{\pi c}{6L} \tag{1.93}$$

Therefore if we know the spectrum under *periodic boundary conditions* the $\frac{1}{L}$ correction to the ground state energy gives us the value of central charge, and the finite gap scaled as $\frac{1}{L}$ yields the conformal weights.
We can summarize it in two different rules:

$$E_0 = \varepsilon_\infty - \frac{\pi c v}{6L} \tag{1.94}$$

$$\Delta E = (E_{mn} - E_0) = \frac{2\pi v}{L}(d_{mn} + N + \bar{N}) \tag{1.95}$$

For the quadratic Hamiltonian of **Luttinger liquid** the conformal charge is $\mathbf{c = 1}$ [11, 14, 21]. Also ε_∞ is the energy of the ground state at infinite length, (N,$\bar{N}$) are the contributions coming from the secondary fields, d_{mn} is the scaling dimension and v is the velocity of the *elementary excitations*, we can think it as a term that takes into account the *anisotropy factor* in the finite size scaling relations.

1.1 Entanglement Entropy

The concept of Entropy was introduced for the first time in Thermodynamics.
A more physical meaning of this quantity comes from *statistichal mechanics*, where thanks to *Ludwing Boltzmann's* works on *kinetic theory*, this quantity has been linked to the probability of the configurations of a thermodynamic system.

$$S = K_b ln(W) \tag{1.96}$$

This is the famous **Boltzmann's Entropy** where K_b is the *Boltzmann constant* and W is the number of all the possible configurations of the system in phase-space.
Afterwards this concept was incorporated in information theory by *Claude E. Shannon* in which it takes the name of **Shannon's Entropy**.
After the developing of quantum theory and the rise of the possibility to communicate using quantum codification of information, the theory was extended to *Quantum Information Theory* and consequently it was rewritten in the quantum paradigm taking the name of **Von Neumann entropy**.
In reality we are interested to another kind of entropy, **Entanglement entropy**, that comes from the *Von Neumann entropy*, but it focuses just on a part of the whole system. This is possible considering the whole system like two sub-systems entangled and considering how they share the information.
The final goal is to define a relation among this quantity and the theories that characterize the phases of the system to obtain an observable useful to the building of the phase diagram.

1.1.1 Classical entropy

Entropy is the key concept of classical information theory, in this context is named **Shannon entropy** and is defined as

$$S_{Sh} = -\sum_x p_x log(p_x) \tag{1.97}$$

where p_x are the probabilities of possible different outcome values that the random variable could take.

We can explain the meaning of entropy by saying that: given "W" as a random variable, the Shannon entropy of "W" measures the amount of uncertainty about "W" before we learn its value.
Equivalently we can say that it is the measure of how much information we have gained after we learn the value of W.
It is important to observe that for each value of the probabilities this function is defined, because

$$lim_{x\to 0} x log(x) = 0$$

The reason to define this quantity is that it can be used to "quantify the resources needed to store information"[29, 32].

1.1.2 Quantum entropy

Before we start to talk about the quantum entropy, we can give a little explanation about the phenomena that dominate this context

Entanglement This phenomenon was introduced for the first time by Einstein, Podolsky and Rosen (EPR) in 1935.
In their paper they proposed a paradox about the behavior of a quantum system divided in two different sub-systems by stating: "*Quantum mechanics theory implies the existence of global states of composite system which cannot be written as a product of the states of individual subsystems*".
It means that both live in a superposition of states that distinguish them. When we observe one of them, the system collapses on one of the possible states, instantly the other system collapses to a different one [29].
Practically if we consider two *entagled* fermions it means that both live in a superposition of spin up and spin down, observing just one of them, it will choose one of the two values of spin. The other particle, independently of the distance, will choose instantly the other outcome.

In the quantum case we will already find the concept of probability intrinsically in the theory. We can define a *density operator* replacing probability distribution.
We can define the **Von Neumann Entropy**

$$S(\rho) = -Tr(\rho \ log_2(\rho)) \tag{1.98}$$

if we develop the trace, we obtain:

$$S(\rho) = -\sum_x \lambda_x log_2(\lambda_x) \tag{1.99}$$

where the λ_x are the eigenvalues of the density matrix. If we consider now a system split in two different sub-parts, so we can define the **total density matrix**

$$\rho = |\psi\rangle \langle\psi| \tag{1.100}$$

that acts on the space

$$\mathcal{H} = \mathcal{H}_a \otimes \mathcal{H}_b \tag{1.101}$$

So we can define the so called **Reduced density matrix** as

$$\rho_a = Tr_b(\rho) \tag{1.102}$$

We can define the **Entanglement Entropy** like the *Von Neumann entropy* just for the reduced density matrix

$$S_a = -Tr(\rho_a) ln(\rho_a) \tag{1.103}$$

Similarly we can do for the system b when ρ corresponds to a pure quantum state $S_a = S_b$.
When a system is in a mixed state the entanglement entropy is no longer a good measure of entanglement. The best way to obtain the entanglement entropy is to construct directly the *reduced density matrix* or at least its eigenvalues λ_i. In our work we obtain directly this information since we are working numerically using a DMRG method [6, 29, 32].

1.1.3 Entanglement entropy in conformal field theory

Using the aforementioned concepts, we can try to introduce a very suitable formula that we can use to observe numerically the characteristic parameters of a theory.
Considering a system close to the quantum critical point, where the correlation length ϵ is much larger than the lattice space (a), the lowlying excitations and the long-distance behavior of correlation in the ground state of a quantum spin chain are believed to be described by quantum field theories in 1+1 dimensions.
At the critical point where the $\epsilon^{-1} = 0$, the field theory is massless, and is a *Conformal field theory.*
Using the methods of the conformal theory it was found [7] that the the **entanglement entropy** has this features:

$$S_A \sim \frac{c}{3} log(l/a) \tag{1.104}$$

where l is the length of an interval in an infinite system.
Considering the case of finite length (L) and for **Periodic boundary conditions**, the above formula has to be changed to [6]:

$$S_A = \frac{c}{3} log\left(\frac{L}{\pi a} sin\left(\frac{\pi l}{L}\right)\right) + c_1' \tag{1.105}$$

where c_1' is a non universal constant [5, 6].
Formula (1.105) is important because it allows the calculation of the central charge c.

Chapter 2

One dimensional model of spinless fermions with softshoulder interaction

Following what has been discussed in literature in recent years, in this chapter we will present a brief review of the model describing *one-dimensional chain of spinless fermions with softshoulder interaction* described inside the works [10, 27] with *periodic boundary conditions* or PBC:

$$H = \sum_{i=0}^{L} t(b_i^\dagger b_{i+1} + b_{i+1}^\dagger b_i) + V \sum_{\substack{i,l=0 \\ |i-j|\leq r_c}}^{L} n_i n_j \tag{2.1}$$

This Hamiltonian is written in second quantization, where the operators $b_i(b_i{}^\dagger)$ are the **fermionic operators of distruction (creation)** that satisfy the commutation relations:

$$\{b_i^\dagger, b_j\} = \delta_{i,j} \qquad\qquad \{b_i, b_j\} = 0$$

The n_i is the **number operator** defined $n_i = b_i{}^\dagger b_i$, this is a "bosonic" operator. The r_c is the *range of potential*, it determines the distance within which two different particles interact. We can see that the Hamiltonian is split in two different parts:

Hopping term It is the first part of the Hamiltonian and it is linked to the *Kinetic Term* that we know from the Hamiltonian Theory. In a more general way this is a matrix and in this case we consider just the hopping between *nearest neighbor* sites and we consider the real parameter (t) as the "energetic cost" of the hopping process.

Potential term The second part of the Hamiltonian defines how particles interact between each others. The strength of interaction is given by the parameter "V" which

we will assume to be positive, giving a repulsive interaction.
In our case the particles interact under a finite length (r_c) potential. This kind of interactions is called *softshoulder*.
From reference [27] we can state that the fermionic or bosonic nature of the particles doesn't influence the description.
This because the low-energy behavior is described by a free bosonic theory.
We will consider closed systems with fixed density that becomes another parameter of the theory ($\bar{n}$).
We notice that the Hamiltonian is particle-hole invariant so that we can define and work with a more suitable quantity:

$$\begin{cases} \rho = \bar{n} & (\bar{n} \leq 1/2) \\ \rho = 1 - \bar{n} & (\bar{n} > 1/2) \end{cases} \tag{2.2}$$

We will consider the case of *Periodical Boundary Conditions* (**PBC**).

2.1 Phase diagram

The $T = 0$ phase diagram of the model (2.1) is shown in figure 2.1, as function of the potential range r_c and the potential coupling V/t. measured in units of t.

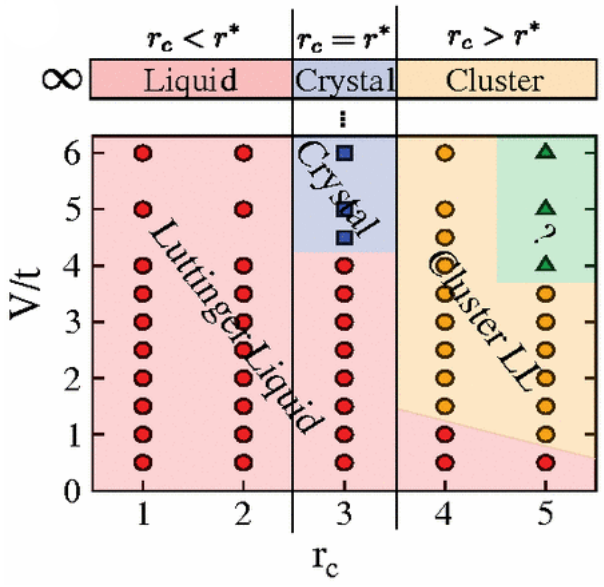

Figure 2.1: Numerical zero-temperature phase diagram of the Eq.(2.1) for density $\bar{n} = 3/4$. Figure taken from [27]

We can define ρ as the density of the particle system and $r^* = \frac{1}{\rho} - 1$ as the *average distance* between two particles.
In the phase diagram given in figure 2.1 it is possible to observe four different phases:

- **Luttinger Liquid**
- **Crystal**
- **Cluster Luttinger Liquid**
- **Unknow**

To understand the phase diagram and its features let's start from the classical case.

2.1.1 Classical case

We define the classical case when we "turn" to zero the hopping term ($t = 0$) or equivalently, when the strength of interaction (V) tends to infinity.

$$V \to \infty \tag{2.3}$$

As we can see from the (2.1) there are three different phases depending on the value of r_c.
Let's start to analyze the Hamiltonian saying that under the condition (2.3) it commutes with the number operator (n_i).

$$[H, n_i] = 0$$

We know from quantum mechanics that in this case they share the eigenstates [9].
We can use them to observe the classical features of each phase.
Let's define a new parameter given by the ratio of critical range and the r^*.

$$C = \frac{r_c}{\frac{1}{\rho} - 1} = \frac{r_c}{r*} \tag{2.4}$$

This parameter gives us information about the organization of the particle inside the lattice independently of its length.
This can be a general way to observe how the phases of system depend on it.

Liquid structure $0 < C < 1$
In this case starting from the definition of the parameter we can say that the mean value of free places is too high compared to the range of interaction, it means that the particles can live "free" to move on the lattice without any increase to the energy, does avoiding to reduce the relative distance under the critical range.
We can show a representation of one of these states

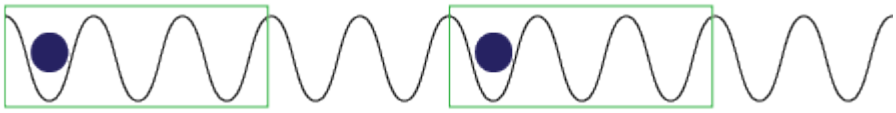

Figure 2.2: Liquid structure with $r_c = 2$, $\rho = 1/5$, $r^* = 4 > r_c$, $C = 1/2$, lattice of L=10. Green boxes are packages of a particle and 2 free spaces.

Cluster Structure $C > 1\,,\ C \notin \mathbb{N}$
Here we can see that to obtain this value the interaction range needs to be bigger than the inter particle distance.
In this peculiar situation, in order to minimize the interaction energy, the particles prefer to "stick together" generating something that is defined **cluster** [10].
The **number of clusters** is given by the following formula:

$$M = \frac{L}{r_c}(1-\rho) \qquad\qquad M \in \mathbb{N} \tag{2.5}$$

Given this definition it is possible to rewrite the C parameter as

$$C = \frac{N_{particles}}{M} \tag{2.6}$$

We have to say that clusters have to respect some particular rules:

- Only two kind of clusters can exist **A**, **B**
- The particles number between the two clusters have to differ by just one element $M_A = \alpha\ ,\ M_B = \alpha + 1$

the first is valid because observing the C value says that there are not enough particles to create all the packages of kind B and too many to create all packages of kind A. These are the only two structures that can minimize the number of interactions. Let's show the relation that defines the clusters in terms of density, derived from the C value:

$$\begin{cases} \alpha = int(C) \\ \rho_B = frac(C) \\ \rho_A = 1 - \rho_B \\ \alpha \leq r_c \end{cases} \tag{2.7}$$

$\rho_{A,B} = \frac{M_{A,B}}{M}$ is the density of cluster of kind A or kind B, int(C) is the integer part of C and frac(C) is the decimal part of C.
We can see an example of cluster formation in lattice

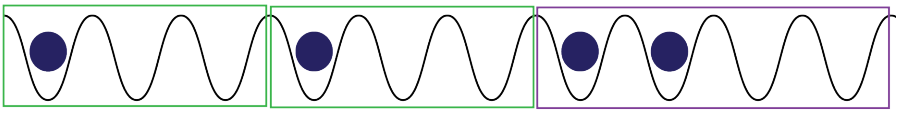

Figure 2.3: Cluster formation with $r_c = 2$, $\rho = 2/5$,$r^* = 3/2 < r_c$, $C = 4/3 = 1.3333$, lattice of L=10. Green boxes for cluster of kind-A, and purple box for cluster of kind-B.

In figure 2.3 there is a case of cluster formation, we can see how the formation of this structure is linked to the parameters (2.7):
$\alpha = 1$ it means that inside the cluster of kind-A we have just one particle, and inside the cluster of kind-B we have two particles.
$\rho_B = 0.33333 = 1/3$: It means that given the total number of cluster (2.5) M=3, we can compute the number of clusters of kind-B ($M_B = \rho_B M = 1$), and the number of clusters of kind-A ($M_B = \rho_A M = (1 - \rho_B)M = 2$).

Crystal structure $C \neq 1$, $C \in \mathbb{N}$
This is a particular case of the previous. In fact when the ratio is an integer number it means that the range of interactions and the average distance are multiple integers.
By the previous statement we can say that in this case there are clusters of just one kind.
We can show a picture of this kind of structure in the next figure:

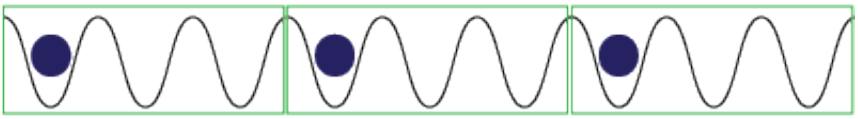

Figure 2.4: Crystal with $r_c = 2$, $\rho = 1/3$,$r^* = 2 = r_c$, $C = 1$, lattice of L=9. Green boxes for cluster of kind-A.

From the figure 2.4 it is possible to observe that the in agreement with the theory if $C = 1$ there are just clusters of kind-A, so the particles are positioned in an periodic structure as it happens in a crystal.

Phase diagram In summary, when $C < 1$, single particles are free to move and we are in a liquid phase of particles, so in a Luttinger liquid. When $C > 1$ but not integer, blocks of particles, the so called clusters, are free to move and hence we are in a liquid phase of clusters, i.e. in a cluster Luttinger liquid. Finally, when $C = 1$, particles are not free to move without interacting strongly, hence we are in a crystal phase. This is shown in figure 2.5.
We extend the definition of "crystal" from being made only of equidistant particles to also include the case in which packages of stuck together particles are equidistant as well.

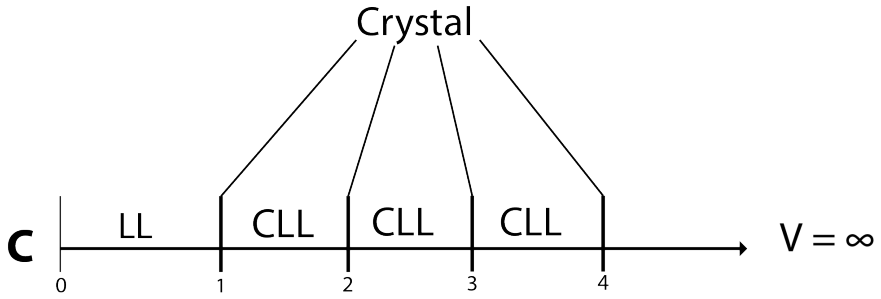

Figure 2.5: Phase diagram for the classic case ($V \to \infty$)

Luttinger liquid and cluster Luttinger liquid To talk about Luttinger liquid it's necessary to treat the quantum case. We "force" the terminology by using the same name in the classical context to mean a *high degenerate state*. We describe it as a liquid whenever we find that it is possible to obtain the same energy with a high number of states (eigenstates in our case). It means that particles are essentially free to move.
For the cluster case, the rising **frustration** in the system induces the degeneracy of a cluster state that we can analytically compute.
Let's show the *degeneration formula*

$$d = \frac{L}{M}\left(\frac{N_T!}{N_A!N_B!}\right)\left(\frac{M!}{M_A!M_B!}\right) \tag{2.8}$$

Defining N_T as the total number of particle in the lattice, N_A, N_B as the number of particles of each species.
Looking at the formula (2.8) we can say that increasing the length of the chain, it will also proportionally increase the number of clusters. So at the thermodynamic limit the degeneration tends to infinity, this allows us to consider the cluster phase as a **liquid of clusters**.

2.1.2 Quantum case

Let us now work with $t \neq 0$, or equivalently $V \ll \infty$.
Now we can try to connect the classical and quantum regime.
When we talk of a liquid with quantum behavior we mean a *Luttinger Liquid*.
We know that this picture holds for both spin and Hubbard-like models with short range interactions [10] thus we can give a proof that this paradigma still holds in our context as well.
Let's show the results obtained from numerical calculation in previous works [10, 27].
We can start to observe the ground state looking at the *structure factor* (1.49) plots produced from the numerical simulations.

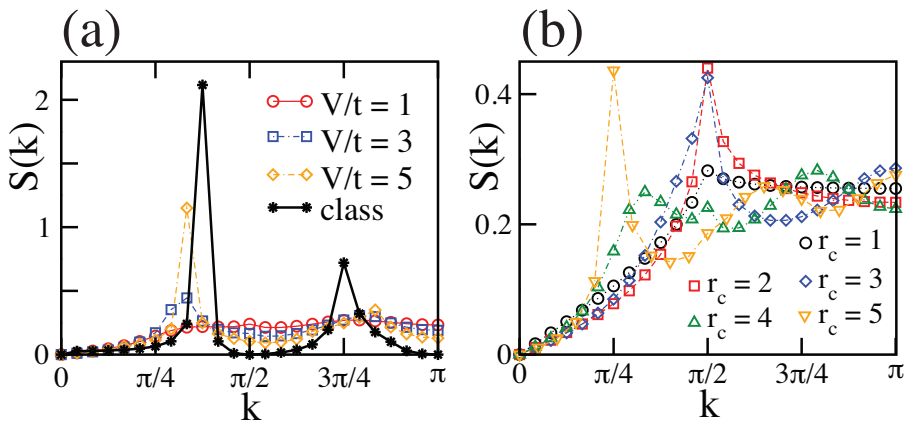

Figure 2.6: (a) Structure factor S(k) at fixed $r_c = 4$ and for several values of V/t for a chain of length L=48 and $\bar{n} = 3/4$.
(b) S(k) for different values of r_c and fixed V/t=1.5 for a chain of L=48 and $\bar{n} = 3/4$.
Figure extracted from [27].

Looking at the graph figure 2.6(b) we see that by varying the values of r_c the peak of the structure factor changes position.
We can recognize that the peaks for $r_c < 4$ are positioned where we expect them from the Luttinger Liquid. As we know from theory the peak is linked to the oscillating part of density-density correlation and the argument of the cosine is exactly the *particle density* times 2π (1.48), so we expect a peak at

$$k_c = 2\pi\rho = 2\pi\frac{1}{4} = \frac{\pi}{2} \tag{2.9}$$

Looking at the graph 2.6(a) we can see that there is a *treshold* under which the peaks disappear, so it has to exist another transition when $t \simeq V$ to a ground state representing a strongly interacting quantum liquid.
We can see that in terms of the classical interpretation, for the given density and range of potential ($r_c \geq 4$,$\rho = 0.25$) we expect the formation of clusters.
Starting from the classical interpretation, that explains the high degeneracy of the ground state, we can derive an **effective Hamiltonian** describing the limit $t \ll V$.
We can do it by defining $\mathcal{P}$ as a *projector operator* on the ground state manifold, and apply conventional sencond order perturbation theory [1, 2].

$$H_{eff} \simeq H_0 + \mathcal{P}H_t\mathcal{Q}\frac{1}{\varepsilon - H_0}\mathcal{Q}H_t\mathcal{P} + \mathcal{O}(t^4/V^3) \tag{2.10}$$

where $\mathcal{Q} = \mathbb{1}$ - $\mathcal{P}$, and ε is the ground state energy.
Now we can define an effective spin-$\frac{1}{2}$ operators ($\tilde{S}_j$) associating the clusters of kind-A

as spin-up and kind-B as spin down.
This is a mapping from the Hilbert space defined by $\mathcal{P}$ to the Hilbert space of a spin 1/2 chain with M sites.
For $r_c = 2$ case, diagonal contributions $(\tilde{S}^z_i \tilde{S}^z_{i+1})$ do not contribute at lowest order [10], so we obtain an *effective Hamiltonian* as shown

$$H_{eff} \simeq H_0 + \frac{t^2}{V} \sum_{j=1}^{M} [(\tilde{S^+}_j \tilde{S^-}_j + h.c.) + 2] \tag{2.11}$$

The **strong coupling limit** can be mapped to a sysem of **Hardcore Bosons** hopping in an artificial lattice created by the underlying cluster structure.
This means that the **Cluster Luttinger Liquid** phase can exist in the ground state of quantum systems as well for strong coupling, and it is described by a c=1 conformal field theory.
This approach works well because we find a good agreement between the exact and the perturbative result above $V/t \geq 5.0$ as it is shown in figure 2.7.

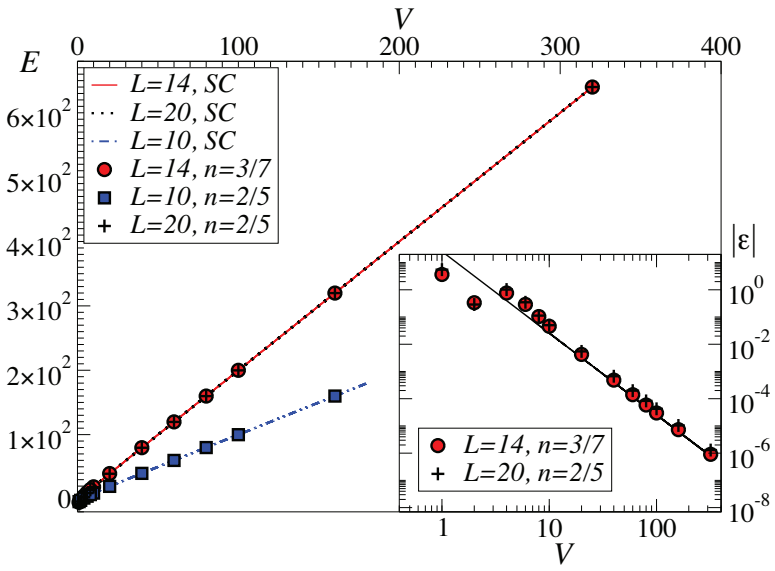

Figure 2.7: Plot of the energy of ground state as function of V/t for different cluster configurations, taken from [10].
Symbols denote the exact energies of the Hamiltonian (2.1) obtained numerically, *lines* show the perturbative calculations according to Hamiltonian (2.1).
The insets is a zoom around the low energy on which is possible to see that the results of the two methods are not in agreement.

From the figure 2.7 we can see a poor agreement below $V/t \geq 5.0$.
It means that for strong coupling the clusters play a role of mesoscopic degrees of freedom. To work at *intermediate coupling* we can see how the constraints given by the clusters can be applied to *phenomenological bosonization* to capture the correct behavior of the *correlation function*.
To do it we start from the first steps of phenomenological bosonization (1.38):

$$\rho(x) = \sum_{n=1}^{N} \delta(x - x_n) = \sum_{n=1}^{M} \delta(x - x_n) + \sum_{l \in cl} \delta(x - x_l) = \sum_{n=1}^{M} f(x_m)\delta(x - x_m) \tag{2.12}$$

where the δ is a Dirac's delta that counts the clusters, and $f(x_m)$ counts the particles per cluster.
We can see that in a different way from the classical bosonization we get the sum split into two parts, where the first one describes the fact that there are some clusters where just one particle lives, while the second term takes into account the possibility of having clusters formed by two particles.
In fact the sum $\sum_{l \in cl}$ represents the sum over all two particles of clusters.
Now we can introduce a new field $\phi_{cl}(x)$, *cluster count field*, which counts the fluctuation of cluster density

$$\phi_{cl}(x) = \phi_{cl}(x + L) + M\pi\,, \quad \phi_{cl}(x_m) = \pi m \tag{2.13}$$

where m is the label of the cluster.
To obtain the correlation function with this kind of field the calculations are practically the same as we have seen in the first chapter so we avoid to repeat them and advise for the interested reader to consult the paper [10].
Let's show just a step where a fundamental piece that we will find in the correlation function is present

$$\phi_{cl}(x) = -2\phi_{cl}(x)' + 2\pi n\sigma x \tag{2.14}$$

where $\phi_{cl}(x)'$ is a convenient field relative to the perfect cluster-crystalline solution, n is the particle density and σ is a cluster density

$$\sigma = \frac{M}{N} \tag{2.15}$$

Thus we obtain the **cluster density field** as shown in the next formula

$$\rho(x) = \left[n - \frac{\sigma}{\pi}\boldsymbol{\nabla}\phi_{cl}(x)'\right]\left\{\sum_{k=-\infty}^{\infty} a_k e^{2ik[\phi_{cl}(x)' - \pi\sigma x]}\right\} \tag{2.16}$$

Using the cluster density field we can compute the *density-density correlation* that will take the form

$$< \rho(x)\rho(0) >= n^2 + \frac{\alpha_1}{x^2} + \frac{\alpha_2 cos(2\pi n\sigma x)}{x^{\gamma_1}} \tag{2.17}$$

where α_1 , α_2 and γ_1 are non-universal coefficients.
We can see that the correlation function presents the same form as in the previous case, the only difference lies in the argument of the cosine, which is the key feature to determine the shift of the peaks.
We can see that in this new form the point where we expect the peak of the structure factor is

$$k_c = 2\pi\sigma n = 2\pi\frac{1-n}{r_c} \tag{2.18}$$

Considering the case shown in figure 2.6 we can see that, for $\rho = 1/4$ and $r_c = 4, 5$ we obtain $k_c = \frac{3}{8}\pi, \frac{3}{10}\pi$ in very good agreement with the data.
We comment now on some other important features that can be obtained.

Correlation function Looking at the plots of the correlation function given in figure 2.8, we can infer that all of them decay algebraically validating the assumption that LL and CLL phases underlying field theories are c=1 conformal.

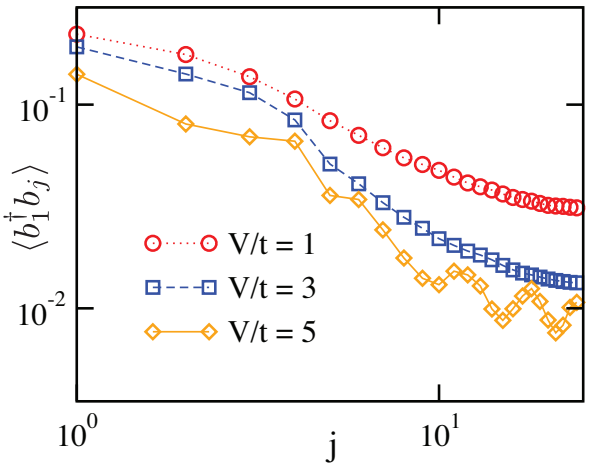

Figure 2.8: Correlation function (log-log scale) for several V/t for $\bar{n} = 3/4$, $r_c = 4$, L=48 sites. Figure extracted from [10]

Luttinger parameters Let's consider three independent ways from which it is possible to extract the Luttinger parameter:
1) expanding the **structure factor** around the low momenta $k \sim 0$ we obtain a relation

$$S(k) \simeq k\frac{2K_L}{\pi} \tag{2.19}$$

2) considering the **level spectroscopy method** [27], utilizing the *scaling of the ground state energy* that we have seen in the first chapter (1.94) we can extract the *sound velocity* (v).
Given the formula

$$K_L = \frac{\pi v}{2G(L)L} + O(1/L^3) \tag{2.20}$$

We can see how it is possible to extract the Luttinger parameter knowing the sound velocity and the *charge gap*.
From the equation (2.20) we can explain that G(L) is the **charge gap** at finite size L (2.21).

$$G(L) = \frac{E_0^{N+1}(L) + E_0^{N-1}(L) + 2E_0^N(L)}{2} \tag{2.21}$$

Where $E_0^N(L)$ is the ground state energy for a chain of length L with N particles inside.
3) considering the **correlation density matrix** [8, 27] for a system with periodic boundary conditions described by a Luttinger liquid theory, it takes the form

$$< b_i^\dagger b_j >= \bar{n} \left(\frac{1}{\bar{n} d_{ij}(L)} \right)^{\frac{1}{2K}} \left[c_0 + \sum_{m=1}^{\infty} c_m \left(\frac{1}{\bar{n} d_{ij}(L)} \right)^{2m^2 K} cos(2\pi m \bar{n} x) \right] \tag{2.22}$$

where c_m are coefficients of the model and $d_{ij}(L) = \frac{L}{\pi}|sin(\pi(i-j)/L)|$ is called *cord length*
Let's observe in figure 2.9 the comparison of the Luttinger parameter for several V/t coming from these three methods.

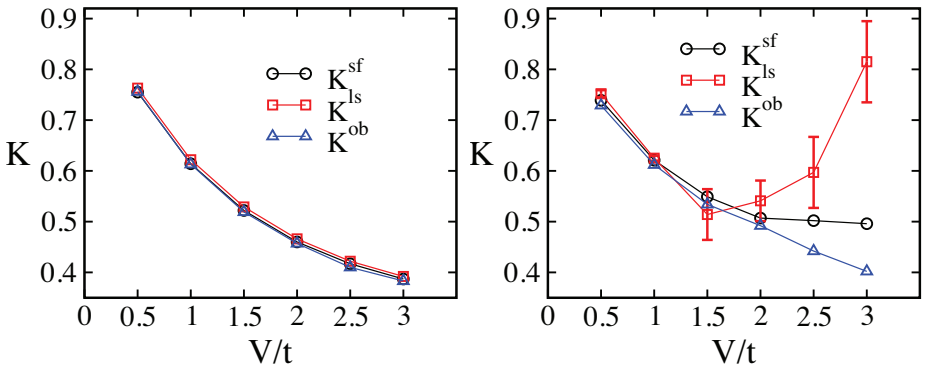

Figure 2.9: Luttinger parameter computed at several V/t for $r_c = 2$ (graph on the left), $r_c = 4$ (graph on the right) for the three aforementioned independent methods.
Figure extracted from [10]

It was verified that the error is smaller than the desired precision K($\sim 10^{-3}$) [27].
We can resume the graphs shown in figure 2.9 saying that for $r_c = 2$ all the methods are

in good agreement; contrarily for $r_c = 4$, in the cluster phase, all three methods agree for low interactions, and differ for the large interactions. We can observe looking at the red error bars shown in figure 2.9 (graph on the right) that the difference among the three methods lives outside it, so we can not justify their differences in terms of the uncertainty of the fit procedure. Other considerations can be done by studying the **Entanglement entropies**.
We can consider the *Calabrese-Cardy* formula (1.105)

$$S_L(l) = \frac{c}{3} ln \left[\frac{L}{\pi} sin(\frac{\pi l}{L}) \right] + C \tag{2.23}$$

where L is the lattice length, l is the block length, C is a non universal constant.
We can linearize it to extract as a slope the conformal charge. We can define a parametrization of the formula as follows

$$S_L(l) = \frac{c(L)}{3} k(l) + a_0 \,, \quad k(l) = ln \left[\frac{L}{\pi} sin(\frac{\pi l}{L}) \right] \tag{2.24}$$

Where the $k(l)$ is the *cord length* introduced before.
We can show some plots of the *entanglement entropy scaling* from which it is possible to extract the conformal charge (c).
Let's see that for the case of $\bar{n} = 4/10$, $r_c = 2$, several lengths and $V/t = 4.0$, shown in figure 2.10(a), we can see that the linear fit of the data has a slope (conformal charge) of c=1.0128. Considering that the finite-size central charge can be extracted with an accuracy of the 1 % we can see that $c = 1.0128 \pm 0.01$ so it is practically one, as expected for a CLL.

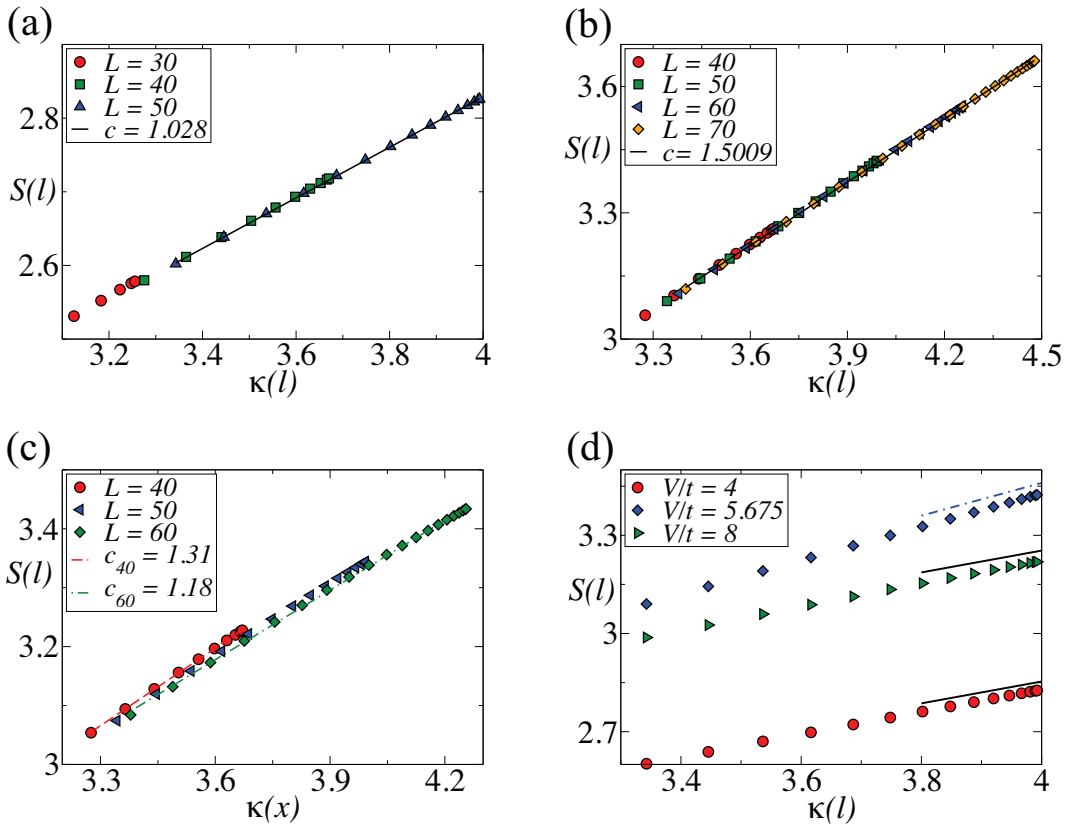

Figure 2.10: Entanglement entropy scaling for $\bar{n} = 4/10$, $r_c = 2$.
(a,b,c) V/t=4.0,5.675,6.5 for several L.
(d) L=50 for several V/t.
Data for different size are indicated by the symbols, while lines are linear fits.
Figure taken from [10].

Analyzing the case of $\bar{n} = 4/10$, $r_c = 2$, several lengths and $V/t = 5.675$, shown in figure 2.10(b), we can see that the conformal charge takes the values $c = 1.5009 \simeq \frac{3}{2}$. Considering the case of $\bar{n} = 4/10$, $r_c = 2$, several lengths and $V/t = 6.5$, shown in figure 2.10(c), we can see that the conformal charge takes the values $c_{40} = 1.31$ for a lattice of L=40, $c_{60} = 1.18$ for a lattice of L=40. It seems that the value of the conformal charge decreases increasing the lattice length.
From the graph shown in figure 2.10(d), where it is represented the case of $\bar{n} = 4/10$, $r_c = 2$, L=50 and several values of V/t, we can observe different slopes.

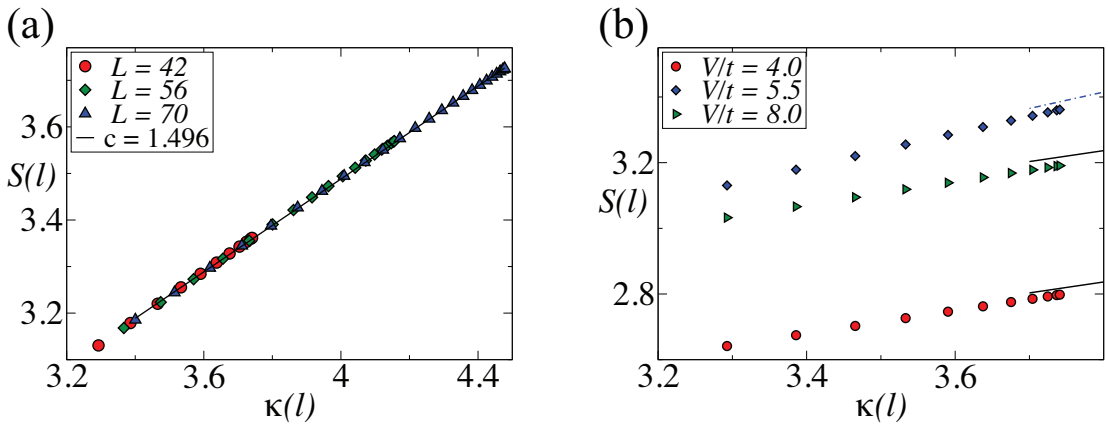

Figure 2.11: Entanglement entropy scaling for $\bar{n} = 3/7$, $r_c = 2$.
(a) V/t=5.5, for several L.
(b) L=50, for several V/t.
Data for different sizes are indicated by the symbols, while lines are linear fits.
Figure taken from [10]

.

We look at the plots shown in figure 2.11 where we consider the case of $\bar{n} = 3/7$,$r_c = 2$. In figure 2.11(a) we can see that for several lengths and $V/t = 5.5$, the conformal charge given by the fit is $c = 1.496 \pm 0.015$, so practically $c \simeq \frac{3}{2}$.
In figure 2.11(b) for L=50 and several interaction strengths we can see that the slopes change. The blue dot-dashed lines say that the the conformal charge takes the value of $c = \frac{3}{2}$. The black continuous line says that the conformal charge is c=1.
Looking at figure 2.12 we can well understand the phase transition linked to the variation of the conformal charge.

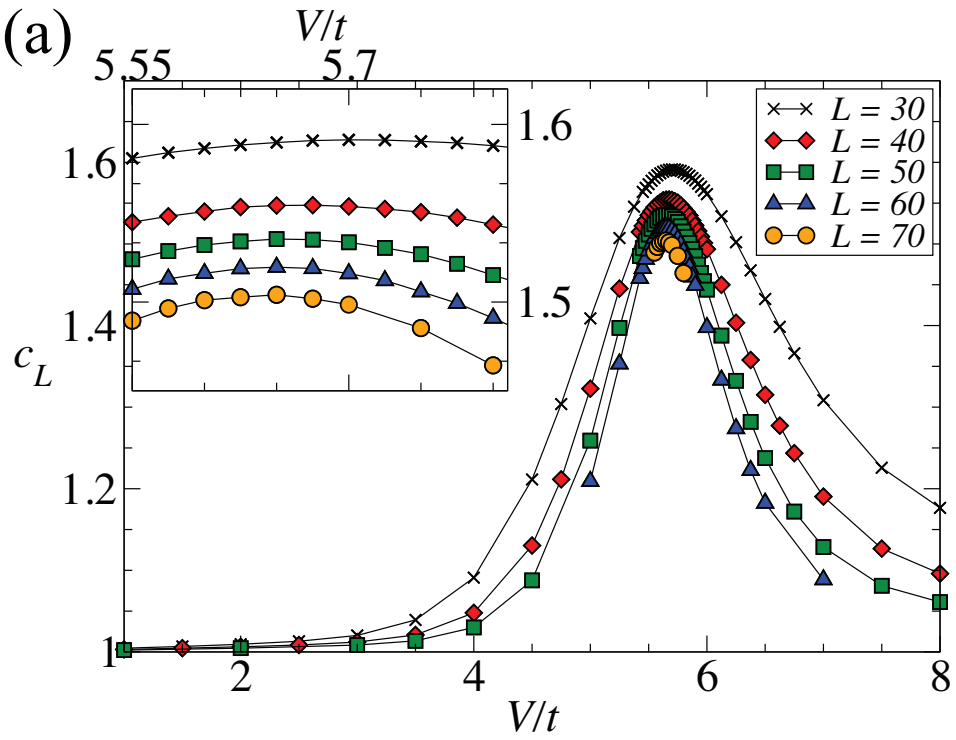

Figure 2.12: Finite-size central (C_L) charge vs V/t.
Figure taken from [10].

In fact we can see that observing the conformal charge plotted for many values of V/t it shows a bell-like structure with a peak of $c = 3/2$ around $V/t \simeq 5.5$, we define it *critical point* ($V^c{}_L/t$).

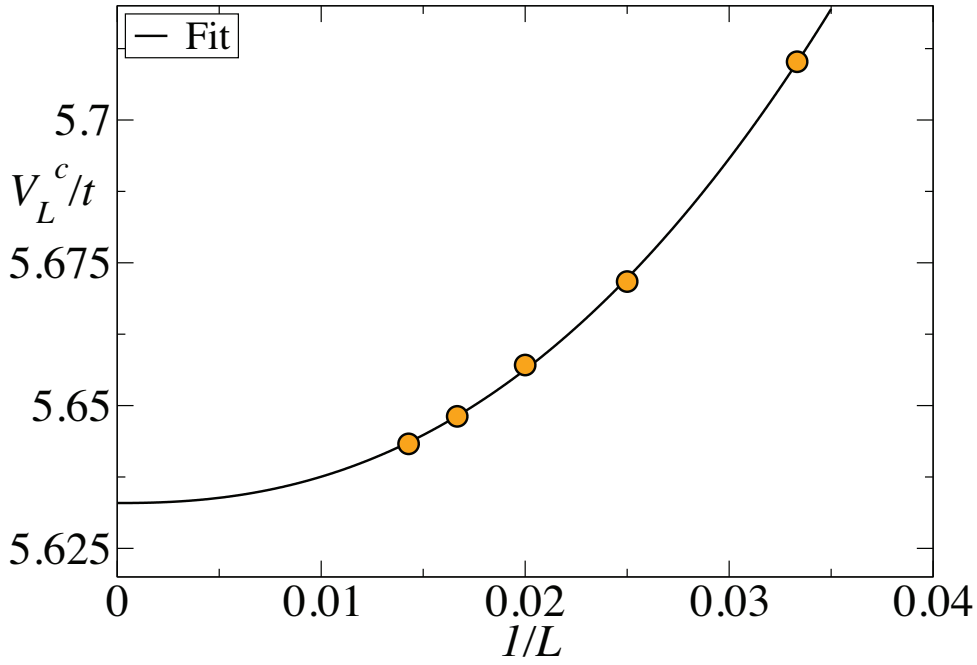

Figure 2.13: Finite-size scaling for the critical point $V^c{}_L/t$ as a function of 1/L. Figure taken from [10].

We can observe from figure 2.13 that the fit of this point says that for infinite length we expect a peak around $V/t \simeq 5.63 \pm 0.02$ with a $c = 3/2$. Let's focalize on another important phenomenon that helps us to understand the low energy excitations near the transition point.
We can define the **single particle gap** as

$$\Delta_{sp}(L) = 2E_N(L) - E_{N-1}(L) - E_{N+1}(L) \tag{2.25}$$

Where $E_N(L)$ is the *ground state energy* in a chain of length L with N particles inside. Furthermore is possible to define the *Cluster gap*, written as

$$\Delta_{cl}(L) = 2E_N(L) - E_{N-2}(L) - E_{N+2}(L) \tag{2.26}$$

We are working with $\bar{n} = 4/10$ and $r_c = 2$ so we expect clusters of these kinds

$$\begin{cases} kind - A & 1\, particle \\ kind - B & 2\, particles \end{cases} \tag{2.27}$$

Let's consider the *classical behavior* for both of them, considering that for lengths $L = 10l$ we expect $N_A = 2l$ and $N_B = l$, where l is an integer number.

Single particle gap Looking at the given structure of the chain, we can see that just the clusters of kind-B contribute to the energy of the system, so our ground state energy is

$$E_N = VN_B = Vl \tag{2.28}$$

As was observed in the article [27] the cost to introduce a new particle in a lattice is $2V$, if we suppress a particle we can see that the energetic gain is $-V$ and it is given by the breakage of a cluster of kind-B. Thus we can write the energy of the doped state as

$$E_{N+1} = Vl + 2V\,, \qquad E_{N-1} = Vl - V \tag{2.29}$$

We can see that in the classical case the single particle gap is open and its value is $\Delta_{sp}(L) = V$ for every system size.

Cluster gap Now we consider the energy cost in order to introduce two particles inside the system, so the amount of particles of a cluster of kind-B.
The energetic cost of the doped system is

$$E_{N+2} = Vl + 3V\,, \qquad E_{N-2} = Vl - 3V \tag{2.30}$$

This is valid only for $l \geq 3$. This could be explained by saying that if we merge three couples of clusters of kind-A to form three clusters of kind-B we gain six places of free space where it is possible to introduce the other two particles in order to form two new clusters of kind-A, with this operation we take an energetic contribution of $3V$, any other configuration is more expensive.
We can explain the other quantity by saying that subtracting two particles we destroy two clusters of kind-B and we gain two free spaces that allow a third cluster of kind-B to be split, in a more economic way, in two clusters of kind-A.
Thus we obtain an energetic gain of $-3V$.
We can see that the *cluster gap* is closed for every lattice length.
Now we can see the behavior in quantum regime for intermediate coupling, and show some numerical results.
From figure 2.14 it is possible to see that the *cluster gap* goes to zero in the thermodynamic limit.

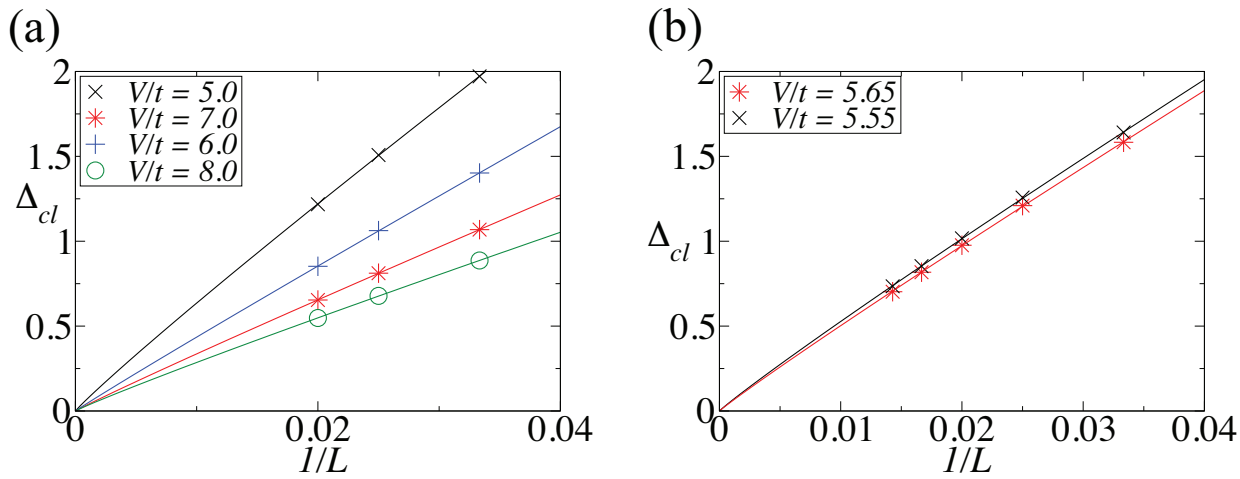

Figure 2.14: Finite size scaling of cluster gap for $\bar{n} = 4/10$ $r_c = 2$ for several values of V/t.
Figure taken from [10]

.

Let's observe from figure 2.14(b) that near the phase transition cluster the gap is closed.

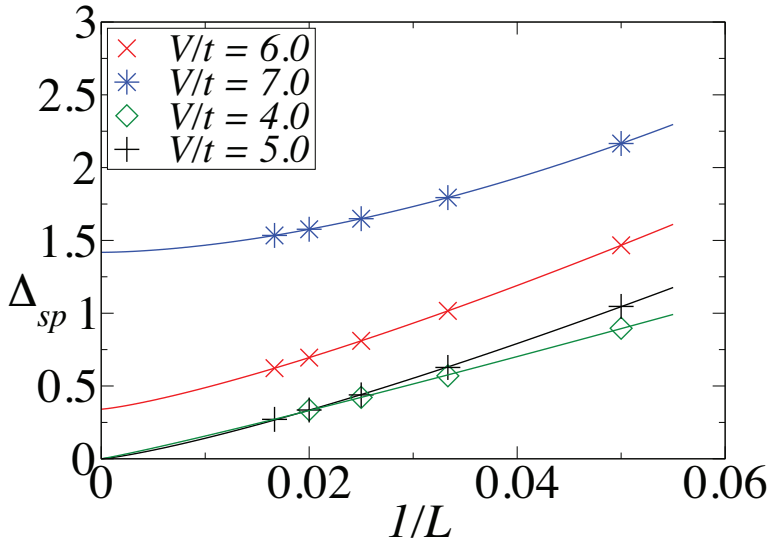

Figure 2.15: Finite size scaling of single particle gap for $\bar{n} = 4/10$ and $r_c = 2$. Figure taken from [10]

.

From the figure 2.15 we can see that above $V/t = 5$ the single particle gap opens while the cluster gap remains closed, there must be a phase transition between CLL and LL. In both graphs sizes below $L = 10$ are excluded in order to avoid finite size effects. To observe in details where the single particle gap opens we can look at the graph shown in figure 2.16.

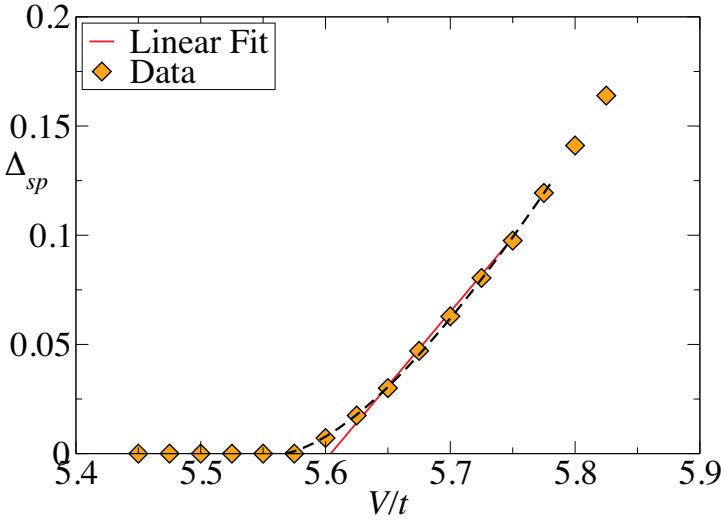

Figure 2.16: Single particle gap extrapolated to the thermodynamic limit as a function of the interaction strength.
Figure taken from [10]

We can see from the graph in figure 2.16 that the Δ_{sp} seems to increase approximately linearly, fitting the non-zero gap we can see that it starts to open at $V/t \simeq 5.6$ and it shows a consistent behavior with an emergent Ising field at the critical point. We can notice that the open of the gap coincides with the phase transition observed from the entropy.
The Authors identified it as a *supersymmetric critical point* where the low energy field theory is described by a combination of a boson and a real fermion (Ising).
Other observations were done on this critical point by computing the bosonic and fermionic *sound velocity*.
Moreover the finite temperature proprieties of the cluster Luttinger liquid state were studied by observing the structure factor at finite temperature.
To read more about these last observations we suggest to read the main work [10]. Other important features are going to be briefly introduced because they are outside the treated theories. Looking at the **excitation spectrum** $\Omega(k)$ in the cluster Luttinger liquid we can see in figure 2.17 the formation and evolution of *roton instability* for increasing interaction.

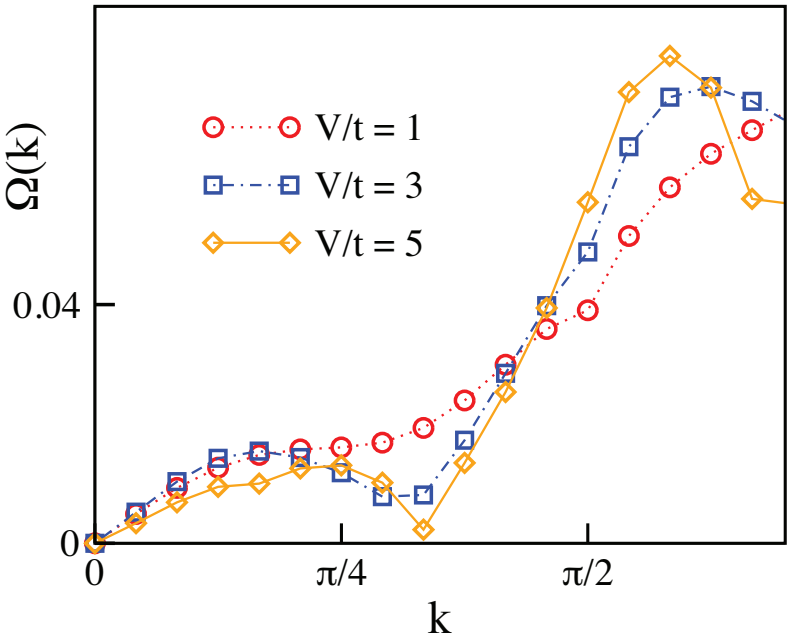

Figure 2.17: Excitation spectrum for $\bar{n} = 3/4$ and $r_c = 4$ and L=48.
Figure taken from [27]

We can see that, increasing the strength of the interaction, the spectrum has a minimum for the same k_c that we have seen in the structure factor.
This minimum tends to zero, so a cluster-like roton minimum instabilities appears with a null roton-gap. Another observation states that the **BKT transition** (Bereziskii-Kosterliz-Thouless) appears at $r_c = 3$ and $\bar{n} = 3/4$.

Chapter 3

DMRG numerical simulation

In this chapter we will analyze the main numerical tool used to produce the results of this work: the powerful **DMRG code**, developed and improved by Professor of the University of Bologna *Fabio Ortolani* and his team, that now is used in many different research teams around Europe.
We will explain the basic concepts of this method and how it works.

3.1 Density Matrix Renormalization Group

The Density Matrix Renormalization Group (DMRG) is a *numerical technique* to find with a good approximation of the ground state and the low-lying excited states of strongly interacting quantum system, such as *Heisemberg, t-J* and *Hubbard* model.
This method works very well in one-dimension, but many researches are trying to expand it towards more dimensions.
Let's first write a brief introduction to few techniques that are propaedeutical to well describe the DMRG method.

3.1.1 Exact Diagonalization

For the majority of interacting systems there aren't controlled analytical methods to treat them, so we need to resort to *numerical techniques*. For lattice models the most direct technique is called **exact diagonalization**: it consists to *diagonalize* directly the Hamiltonian matrix.[31]
We recall that all the possible configurations of the system generate a space called **Hilbert space**.
A convenient basis for the Hilbert space has the form

$$|1\rangle \otimes |2\rangle \otimes |3\rangle \otimes \cdots \otimes |n\rangle \tag{3.1}$$

where $|i\rangle$ is an element of the basis of a single site, and $\otimes$ is the *direct product*.
We can describe an operator that acts on these states like a matrix

$$\hat{A} = A_{i,j} \tag{3.2}$$

where the indices (i, j) define the sites between which the operator acts; a single site operator could be described in the simple form

$$\langle n| \dots \langle 1| \hat{A} |1'\rangle \dots |n'\rangle = \delta_{1,1'} \dots \delta_{i-1,i'-1} \dots \delta_{n,n'} A_{i,i'} \tag{3.3}$$

Efficient methods to diagonalize large matrices and find the spectrum of eigenvalues are **Lanczos method** [23] and **Davisson method** [37].
These methods build up a small set of basis vector and minimize the energy within this basis. The reduced set of basis vectors is systematically expanded until convergence is reached.
Although these diagonalization algorithms work very well with very large matrix (o($10^6 \times 10^6$)), the size of the system that can be treated is limited by the exponential growth of the Hilbert space. The next method that we will describe tries to fix this issue.

3.1.2 Numerical Renormalization Group

For very large systems, it is necessary to formulate a **variational** diagonalization scheme that use a *truncated Hilbert space*, where the truncation is made in a controlled way.
The basic idea of NRG is to progressively integrate out unimportant degrees of freedom, using a succession of renormalization group transformations [31].
The method consists in: first giving a representation of the Hamiltonian in a particular basis, afterwards adding degrees of freedom and making a RG transformation and finally transforming the Hamiltonian on the reduced basis.
The NRG algorithm works following several steps:

1. Take a goup of L sites, L has to be small enough so that H_L can be diagonalized exactly.

2. Diagonalize H_L exactly, with one of the previus methods, finding its eigenvalues and eigenvectors.

3. Write the Hamiltonian diagonalized in terms of the new basis

   $$\bar{H}_l = {O^\dagger}_L H_l O_L$$

   where O_L is an ortogonal matrix

4. Add to $\bar{H_L}$ another site to form H_{L+1}

5. Repeat the previus steps using properly the previous bases.

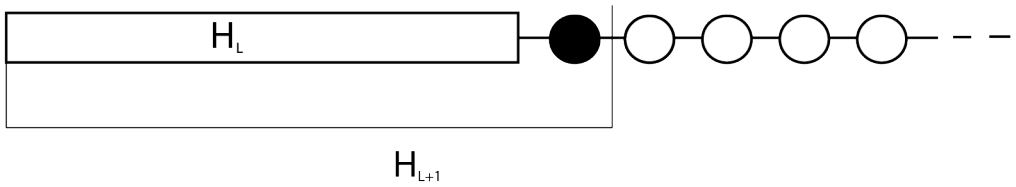

Figure 3.1: picture of Wilson numerical algorithm
figure taken from [31]

The basic idea of this method is that only the the *low-energy eigenstates* obtained for a system of size L will be important in making up the low-energy states of a system of size L=1.
Although this algorithm was carefully presented and justified by Wilson, that calculated the error and compared the numerical results with the analytical one, in a few cases applying this method to Heisemberg or Hubbard model the accuracy becomes quite poor [31].

3.1.3 Density Matrix Renormalization Group

This method is a numerical procedure which works by selecting an optimal subspace of the complete *Hilbert space* according to a different criterion.
Until now it is the most powerful tool to treat one dimensional quantum systems, and this is due to the high precision like ten decimal place for *ground state energy*.

Density matrices We can study a quantum system including the environment around it.
In this way we can write a general system as

$$|\psi\rangle = \sum_{i,j} C_{ij} |\phi_i\rangle |\theta_j\rangle \tag{3.4}$$

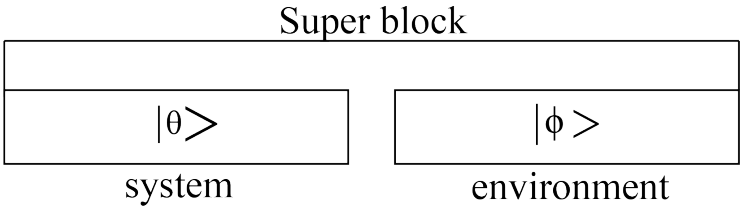

Figure 3.2: A super block divided into a system block and an environment block.

We can say that $|\phi_i\rangle$ is a complete set of vectors in the vector space describing the system, and $|\theta_j\rangle$ is a complete set for the environment as it can be represented in figure 3.2.
We can see that if we consider an operator $\hat{A}$ and we apply it on the aforementioned state, we get:

$$< \hat{A} >= \langle\psi| \hat{A} |\psi\rangle = \sum_{i,i'} \langle\phi_i| \hat{A} |\phi_{i'}\rangle \rho_{ii'} \tag{3.5}$$

where we have introduced the **density matrix** as

$$\rho_{i,i'} = \sum_j C^*{}_{ij} C_{ji'} \tag{3.6}$$

We know that density matrix is an hermitian operator, so for the *spectral theorem* it admits a complete basis of eigenvector and it can be written

$$\sum_{i,i'} \langle i| |i'\rangle = \delta_{i,i'} \quad \sum_{i,i} |i\rangle \langle i| = \mathbb{1} \rightarrow \rho = \sum_i w_i |i\rangle \langle i|$$

with

1. $w_i \geq 0$
2. $\sum_i w_i = 1$

Another important feature is that the average of an operator on the state can be written as

$$\langle\psi| A |\psi\rangle = Tr[\rho A] = \sum_i w_i \langle i| A |i\rangle \tag{3.7}$$

Depending on the value of the "w_i" we can distinguish two kinds of states.
We have a pure state when just one of these w_i is 1 and all the others are 0.
We have a mixed state when more than one w_i's are different from zero.
DMRG considers a quantum system divided into two subsystems that lives in a **pure**

state.
We can say that this method is a **variational** method in a certain state class. Contrary to other variational techniques (e.g. Montecarlo), it doesn't suffer from fermionic sign problem, in fact it can be applied to bosonic and fermionic systems [26].
We can see that there are two different DMRG algorithms, and they are the *finite and infinite algorithm*.

Infinite and finite algorithm

The infinite algorithm consists in increasing, step by step, the length of the system until a precise fixed size is reached, as shown in figure (3.3).

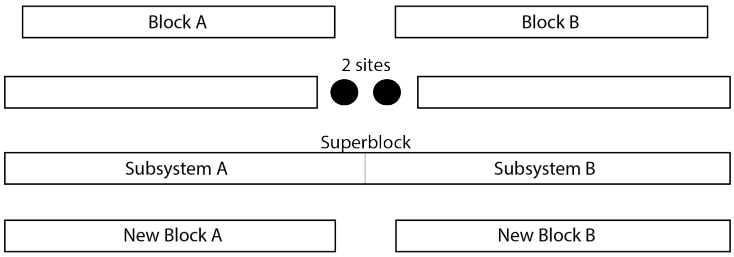

Figure 3.3: Iteration taken in the infinite algorithm DMRG procedure.

Obviously after some short lengths, that is possible to treat exactly, it is necessary to start a **decimation procedure** that consists in taking just a part of the whole *Hilbert space*, so a reduced state space, which can be enough to describe the relevant physics.
This algorithm proposes a method to identify this relevant part and reduce the error on the description of the state in function of the *DMRG states considered*. Let's show how this method works.
We consider a quantum lattice system with L sites labelled by n=1, ..., L.
We define the local space per site

$$\mathfrak{B} = \{|s_n\rangle \, ; s_n = 1, \ldots, d_n\} \tag{3.8}$$

Now we can write the Hilbert space of the whole chain as

$$\mathfrak{H} = \{|\mathbf{s}\rangle = |s_1, \ldots, s_L\rangle = |s_1\rangle \otimes \cdots \otimes |s_L\rangle \, ; s_n = 1, \ldots, d_n\} \tag{3.9}$$

For example for the spin-half Heisenberg model $d_n = 2$ and $\mathfrak{B} = \{|\uparrow\rangle \, , |\downarrow\rangle\}$ [20].
We can write the most general pure quantum state on a lattice as

$$|\psi\rangle = \sum_{\mathbf{s}} c_{\mathbf{s}} \, |\mathbf{s}\rangle \tag{3.10}$$

We can express all the coefficients (c_s) using the **Singular value decomposition** [3], thanks to this formalism we can express all this serie of coefficients as product of matrices (**MPS**) *Matrix Product State* [35].
These matrix will take a different form in function of the *boundary condition*.
We can consider for example the case of *periodic boundary conditions* as shown in (3.11), we can see that all the matrices have the same dimension.

$$PBC \quad (d^{L/2} \times d^{L/2}) \dots (d^{L/2} \times d^{L/2})$$

$$|\psi\rangle = Tr[M^{s_1} M^{s_2} \dots M^{s_L}] \, |\bar{s}\rangle \tag{3.11}$$

For the case of *open boundary conditions* we can say that the we have to consider rectangular matrices, the dimension of which depends on the position respect to the center of the chain [35]. Each matrix is linked to an element of the chain.
The dimension of each matrix for each site increases depending on the length of the lattice and it is impossible to store and manipulate all these matrices.
It's here that we act choosing just a reduced number of states that we will call **D**.
This number goes from o(100) to o(1000) [34, 36].
Obviously increasing the number of the states the precision increases, but meanwhile the time needed to obtain results increases as the numerical error that could deviate the results. So we have to find the right way to choose a sufficient number of them.
We do so by using a Schmidt decomposition [36] that allows us to write:

$$|\psi\rangle = \sum_{a_i}^{r} w_{a_i} \, |a_i\rangle_A \, |a_i\rangle_B \tag{3.12}$$

where **r** is named *Schmidt rank*.
With the truncation we take just a little portion of these r coefficients, more specifically we keep only the states with the r most probable states. Many times they are enough because the weight of these coefficients decays exponentially, so the truncation doesn't influence too much the precision.
Let's see how the growth mechanism works, shown in figure (3.3).
We can describe the state $|a_i\rangle$ using the known states $|a_{i-1}\rangle$ and the basis $|s_i\rangle$ of the additional site:

$$|a_i\rangle = \sum_{a_{i-1}} |a_{i-1}\rangle \langle a_{i-1}| \sum_{s_i} |s_i\rangle \langle s_i| \, |a_i\rangle \tag{3.13}$$

$$= \sum_{a_{i-1}, s_i} \langle a_{i-1}| \langle s_i| \, |a_i\rangle \, |a_{i-1}\rangle \, |s_i\rangle = \tag{3.14}$$

$$= \sum_{a_{i-1}, s_i} A^{s_i}{}_{a_{i-1}, a_i} \, |a_{i-1}\rangle \, |s_i\rangle \tag{3.15}$$

where the matrix $\mathbf{A^{s_i}_{a_{i-1},a_i}} = \langle a_{i-1} s_i | \, | a_i \rangle$ will join the others to describe the increased state, and gives the connection between MPS and block growth $i - 1 \to i$.
The next step of the algorithm is to find the best representation of the true state, this process is a minimization of $|| \, |\psi\rangle - |\bar{\psi}\rangle \, ||$ respect to $|\bar{\psi}\rangle$, where $|\psi\rangle$ is the whole state and $|\bar{\psi}\rangle$ is the approximated state.
This is a highly non linear optimization problem, but it can be done iteratively and linearly as follows:
Starting with an initial guess for $|\bar{\psi}\rangle$, we sweep through the set of matrices, site by site, keeping all others fixed.
Repeating this sweep through the matrices several times it will lead to a convergent optimal approximation.

Finite algorithm

This method can be defined as a *variational ground state search* in the ansatz space of D-dimensional MPSs.
It works to find the ground state, that consists of minimizing the equation

$$\langle \psi | \, \hat{H} \, | \psi \rangle - \lambda \langle \psi | \psi \rangle = 0 \tag{3.16}$$

where $|\psi\rangle$ is the guess ground state, H is the Hamiltonian and λ is the guess eigenvalue.
This is a *nonlinear problem* that in terms of MPS matrix is not directly solvable, anyway it can be divided into a sequence of *linear problems*, their solutions will lead to an iterative improvement of the solution.
The algorithm tries to find every time a lower energy, it means that this method **converge by above**.
Let's show using a picture how this algorithm works

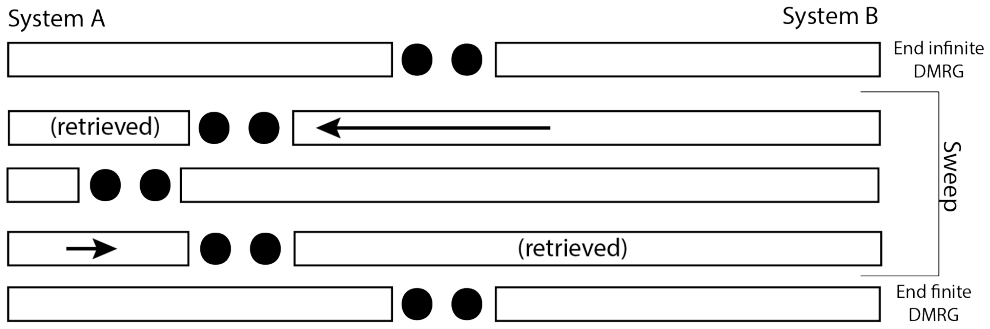

As it is possible to see looking at figure, starting from an entry state that sometimes is given by the *infinite algorithm*, it rewrites and improves the matrices step by step increasing the amount of right normalized matrices that can be thought representing the

system B: this is called *right sweep*. After it repeats the same operation, but using the left normalized matrices that can be thought representing the system A: this is called *left sweep*.
This operation can be made multiple times, until the convergence is reached.

Limitation of the DMRG algorithm

The principal question linked to this method is *how a quantum state can be approximated by MPS*.
In fact, considering the state expressed in terms of reduced density matrix, in a way that $|\psi\rangle$ is normalized, then the eigenvalues w_a of ρ_A are positive and their sum is one.
We have to understand what is the trend of these values and if there is something as a *cut-off*, so an amount of weights that are relevant and a large set of negligible terms.
We can say that for **one-dimensional gapped systems** the eigenvalues $\mathbf{w_a}$ generally **decay exponentially fast**.
In this situation the DMRG method works very well.
A good indicator of precision is the **von Neumann entanglement entropy**, that have to be *not extensive* but proportional to the dimension of boundary of the phase for the ground state of short-range Hamiltonians with a gapped phase [36].
When that is verified, in the one dimensional case the *entanglement entropy* have to be constant.
Instead in critical phases in one dimension a much richer structure emerges. This involves the presence of **logarithmic corrections** ($S(L) \propto log(L)$).

3.2 The DMRG program

Here we try to provide a little sketch about the implementation of DMRG that is used in Bologna.
This code can be divided in two connected parts: a first where it works an *infinite algorithm* and a second part where it works a *finite algorithm*. These two parts are connected because the second step starts from the results of the first, as it is suggested by [36].
Let's start to explain how it works, describing from the input to the output what's happen step by step.
The step zero consists of providing an input file where it is described the Hamiltonian and all the requests are given.
This input file has to be written following a particular syntax, Fortran-like, that the creator of the code has implemented.

The quantities that have to be defined are:
- the parameters of Hamiltonian as the (L) length of the chain;
- the strength of the hopping part (t);
- the strength of the interaction (V) and in our case the range of potential (r_c).
- the description of the one site states specifying their nature (bosonic, fermionic), by writing just one of the creation-annihilation matrix.
Given just one operator and defined the one site states, it is possible to proceed to write the Hamiltonian.
The description of Hamiltonian takes place implementing finite cycles (do) that represent the sum over the index where inside there are the operators, written in terms of product of destruction-creation operators, and the parameter linked to the strength of the action.
The other important thing that has to be inserted is the "target" that is linked to the symmetries, with this command we explain to the code how proceeding to build the state preserving the conserved quantities.
It is also possible to obtain the spectrum of some observables computed on the found states. Moreover it is possible to define the number of DMRG states by requiring a given threshold of precision. Using an opportune key word and writing the Hamiltonian in a proper way, it is possible to fix the boundary conditions.
Now we start to consider, given the input file, how the code runs.
Essentially it works like we explained in the first section, it could be interesting only to specify that it utilizes the *Lanczos method* to diagonalize numerically the Hamiltonian, and another fascinating propriety is linked to the "selection process" used to choose the best value in the given range of DMRG states.
In fact it uses two different criterions: the first consists in calculating the distance between different eigenvalues of the density matrix, and the second is to measure the weight of the excluded part of the state.
This double procedure is necessary to avoid that the algorithm truncates in the middle of a plateau of degenerate states.

3.2.1 Benchmark of input file

The code used in Bologna doesn't need a complete benchmark because of so many papers produced with it.
Anyway, for didactical reasons and to test the good implementation of Hamiltonian, it was performed an *exact diagonalization* for few sites to make a cross reference between them.
It was utilized a not optimized but enough instructive algorithm, that helped to start to understand what are the operations that an exact code have to make.
We implemented an algorithm that creates the **Hamiltonian matrix** and after we *diagonalize it exactly*, finding the eigenvectors and the eigenvalues. Let's start to describe the theoretical concept.

The first step consists in writing the operator in a good basis, this is a crucial step because the implementation of all the chain depends on the implementation of just one site.
We know that we are working in second quantization framework, so really the only operator that we have to define is the **creation/destruction** operator; from this one it is possible to obtain all the operators that we can use.
Let's start to define it considering the action of the operators on the state

$$\begin{aligned} a_A |0_A, 0_B\rangle = 0 \quad &, \quad a_A |1_A, 0_B\rangle = |0_A, 0_B\rangle \\ a_A |0_A, 1_B\rangle = 0 \quad &, \quad a_A |1_A, 1_B\rangle = |0_A, 1_B\rangle \\ a_B |0_A, 0_B\rangle = 0 \quad &, \quad a_B |1_A, 0_B\rangle = 0 \end{aligned} \tag{3.17}$$

$$a_B |0_A, 1_B\rangle = |0_A, 0_B\rangle \,, \quad a_B |1_A, 1_B\rangle = |1_A, 0_B\rangle \tag{3.18}$$

In the same way it is possible to write the relation for the creation operator.
Now we can try to implement the operator using the matrix formalism

$\hat{a}_A$	$\|0_A 0_B\rangle$	$\|1_A 0_B\rangle$	$\|0_A 1_B\rangle$	$\|1_A 1_B\rangle$
$\langle 0_A 0_B\|$	0	1	0	0
$\langle 1_A 0_B\|$	0	0	0	0
$\langle 0_A 1_B\|$	0	0	0	1
$\langle 1_A 1_B\|$	0	0	0	0

where we have to imagine that the operator acts on the states that label the column and after the application these states make a product the states that label the raw.
To describe the B operator it is important to define an important propriety that have to be considered during the construction of the *Fock space*: this is the *order of the operators*. This feature is negligible for the bosons, but is fundamental for the fermions because we have to consider the relative position when the operators act on the state to respect the anti-commutation relation.
We use the order defined by

$$|\psi\rangle = \prod_{\bar{j} \in \mathfrak{B}} a^\dagger{}_{A,j_1} a^\dagger{}_{B,j_2} |0, 0\rangle \tag{3.19}$$

where $\mathfrak{B}$ is the set of all the possible combinations of filled positions, and $\bar{j}$ is just one of there.
Using this order we can write the operator per site

$\hat{a}_B$	$\|0_A 0_B\rangle$	$\|1_A 0_B\rangle$	$\|0_A 1_B\rangle$	$\|1_A 1_B\rangle$
$\langle 0_A 0_B\|$	0	0	1	0
$\langle 1_A 0_B\|$	0	0	0	-1
$\langle 0_A 1_B\|$	0	0	0	0
$\langle 1_A 1_B\|$	0	0	0	0

This description is true and easy to build the one site chain, but to construct the operator that has to act on a long chain is too difficult to write in this way.
For this reason we can show that using the **spin matrix** it is possible to build, using just the *tensor product*, each state.
Given the **Pauli matrices**

$$\sigma_{i=1,2,3} = \begin{bmatrix} 0 & 1 \\ 1 & 0 \end{bmatrix} = \begin{bmatrix} 0 & -i \\ i & 0 \end{bmatrix} = \begin{bmatrix} 1 & 0 \\ 0 & -1 \end{bmatrix} \tag{3.20}$$

From these we can construct the **spin ladder**

$$\sigma^+ = \sigma_1 + i\sigma_2 = \begin{bmatrix} 0 & 1 \\ 0 & 0 \end{bmatrix} \tag{3.21}$$

$$\sigma^- = \sigma_1 - i\sigma_2 = \begin{bmatrix} 0 & 0 \\ 1 & 0 \end{bmatrix} \tag{3.22}$$

it is easily possible to see that these are the creation and destruction operators per site of one specie of fermions and bosons.
Using the **tensor product** it is possible to obtain the operators for two fermions

$$a_A = \mathbb{1} \otimes \sigma^+ = \begin{bmatrix} 0 & 1 & 0 & 0 \\ 0 & 0 & 0 & 0 \\ 0 & 0 & 0 & 1 \\ 0 & 0 & 0 & 0 \end{bmatrix} \tag{3.23}$$

$$a_B = \sigma^+ \otimes \sigma^3 = \begin{bmatrix} 0 & 0 & 1 & 0 \\ 0 & 0 & 0 & -1 \\ 0 & 0 & 0 & 0 \\ 0 & 0 & 0 & 0 \end{bmatrix} \tag{3.24}$$

We used the σ_3 to implement the *anti-commutation relation* that practically consists in counting with a minus the odd number of permutations that have to be done to apply

the operator on the state.
It is possible to make a calculation to find a proof that the anti-commutation relations are preserved.
Now we can write the more general operator for a chain of length L as

$$C_{A,i} = (\mathbb{1}_{A,1} \otimes \mathbb{1}_{B,1}) \otimes \cdots \otimes (\mathbb{1}_{A,i} \otimes \sigma^{+}_{B,i}) \otimes (\sigma^{3}_{A,i+1} \otimes \sigma^{3}_{B,i+1}) \otimes \ldots (\sigma^{3}_{A,L} \otimes \sigma^{3}_{B,L}) \quad (3.25)$$

$$C_{B,i} = (\mathbb{1}_{A,1} \otimes \mathbb{1}_{B,1}) \otimes \cdots \otimes (\sigma^{+}_{A,i} \otimes \sigma^{3}_{B,i}) \otimes (\sigma^{3}_{A,i+1} \otimes \sigma^{3}_{B,i+1}) \otimes \ldots (\sigma^{3}_{A,L} \otimes \sigma^{3}_{B,L}) \quad (3.26)$$

where $\mathbb{1}$ is 2×2 identity matrix.
Using these operators it is possible to implement every fermionic Hamiltonian.
We implemented this Hamiltonian on a *Python script* using the library **NumPy**.
We solved exactly just for four sites.
We can say that because this algorithm store in the memory all the matrix and all the vectors; we know that the dimension of the matrix increases like $(d^{2L} \times d^{2L})$ where L is the length of the chain and d=2.
Anyway our check was positive, so we have observed that for two different methods of exact solving, we found the same results.

3.3 Some results for the one-dimensional one-species model

Here we will discuss the results coming from the reproduced calculation about the one-dimensional model of the last chapter.
We will consider just a little portion of the phase diagram, we made some simulations for $r_c = 2, 3, 4$ for $V/t = 5.0$ for density $\bar{n} = 1/4$ with a not too high precision (200-300) DMRG states.
From the previous considerations here we expect the CLL phase for $r_c = 4$, the LL phase for $r_c = 2$ and the crystal phase for $r_c = 3$. We can observe that the theory is verified looking at the **structure factor**.
Let's show the plots

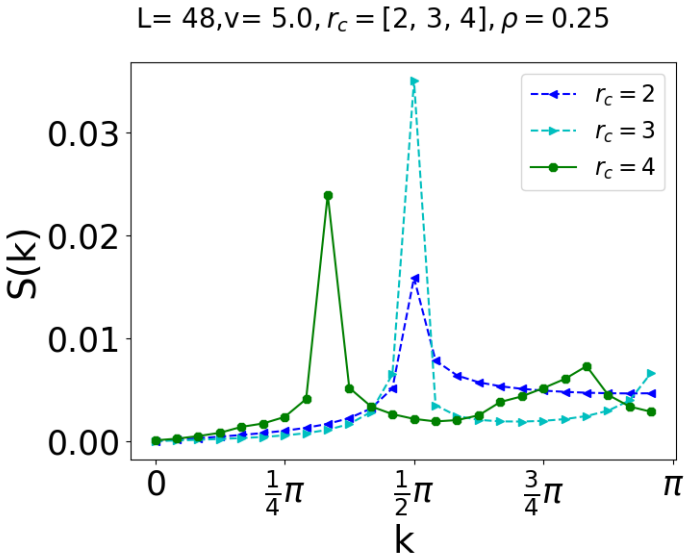

Figure 3.4: Structure factor for $r_c = 2, 3, 4$, $V/t = 5.0$ and density $\bar{n} = 1/4$

From figure it is possible to see that for $r_c = 2, 3$ the peak is positioned at $k_c = \pi/2$, for $r_c = 4$ the peak is shift in $k_c = 3\pi/8$ finding a good agreement with results found by the authors [27].

Chapter 4

Extended Hubbard model with soft shoulder interaction

In this chapter we will treat some aspects of the main model of this work. It is the *Extendend Hubbard model with soft-shoulder interaction*.
It can be seen as the extension of the model discussed before (2.1), where we substitute spinless fermions with two fermionic species.
In this chapter we provide an explanation as regards a little part of its phase diagram.
This part is the innovative contribution given by this work because this model has never been studied until now.

4.1 The model

We can start to write down the Hamiltonian of the *Extended Hubbard model with soft-shoulder interaction*:

$$H = -t \sum_{\substack{i=0 \\ \sigma=A,B}}^{L} ({c^\dagger}_{i,\sigma} c_{i+1,\sigma} + h.c.) + U \sum_{i=0} n_{i,A} n_{i,A} + V \sum_{\substack{i,j=0 \\ 0<|i-j|<r_c \\ \sigma,\sigma'=A,B}} n_{i,\sigma} n_{j,\sigma'} \qquad (4.1)$$

$$\{{c^\dagger}_{i,\sigma}, c_{j,\sigma'}\} = \delta_{i,j}\delta_{\sigma,\sigma'} \quad , \quad \{c^\dagger_{i,\sigma}, c^\dagger_{j,\sigma'}\} = 0 \quad , \quad n_{i,\sigma} = {c^\dagger}_{i,\sigma} c_{i,\sigma}$$

where the $c_{i,\sigma}$ is the annihilation operator for the species $\sigma = A, B$, and $n_{i,\sigma} = {c^\dagger}_{i,\sigma} c_{i,\sigma}$ is the number operator.
We can explain that U, V are two different parameter: the first to define the interaction between two different particles in the same site, the second to define interaction between two particles that live in different sites until a maximum distance called *critical range* (r_c).
In this work we will treat just a limit case, that we will call **one-species limit**.

This name comes considering the limit case $U \to \infty$, where the particles of the ground state prefer to live in different sites and to avoid to live in couple on the same site.
Let's start to explore the *classical behavior* as we made for the one species case.

4.2 Classical behavior

As in the first chapter, we will start from the case where $V \to \infty$. We know that under this condition the Hamiltonian commutes with number operator of each species ($n_{i,\sigma}$), where σ is the label of the species, as shown in figure (4.2).

$$[H, n_{i\sigma}] = 0 \tag{4.2}$$

It means that the Hamiltonian and $n_{i,\sigma}$ share the eigenvectors. As for the previous model (2.1) it is possible to define the quantity $r^* = (\rho_T - 1)$, where $\rho_T = \rho_A + \rho_B$ and (ρ_A, ρ_B) are the densities of each species.
Considering just the total density, we can define a parameter $C = \frac{r_c}{r^*}$ in function of which it is possible to observe features of the classical ground state, like we have done for the one-species model.
As we will see, the situation looks very similar to the one-species model (2.1), so we expect three different phases **Luttinger liquid, Crystal, Cluster Luttinger Liquid**.

4.3 Quantum behavior

Let's go to consider the features of the system for a finite value of the interaction (V). As suggested from the one-species model (2.1) we can try to describe the low energy propriety using the bosonization that allows us to reformulate our model into a free bosonic theory.
To do it let's start to consider the bosonization process for the two species case [14].

4.3.1 Bosonization for two species

If we consider an Hamiltonian where the particles of different species don't interact we can use the boson representation for each spin species separately and we can introduce two sets of fields (ϕ_A,θ_A) and (ϕ_A,θ_B) in terms of which is possible to write the kinetic part of the Hamiltonian as (4.3)

$$H_{kin} = {H^0}_A + {H^0}_B \tag{4.3}$$

where the H^0 is the quadratic Hamiltonian (1.26). In this case the two Hamiltonians are separated from the beginning, so we can treat each one separately obtaining two

different liquids linked to each species.
If we consider two interacting species the interactions are given by all the processes which are given in figure 1.5. We can see the g_4 and g_2 for two species in (4.6,4.5)

$$H_4 = \int \mathrm{d}x \sum_{\substack{r=R,L \\ \sigma=A,B}} \left[\frac{g_{p,4}}{2} \rho_{r,\sigma}(x)\rho_{r,\sigma}(x) + \frac{g_{o,4}}{2} \rho_{r,\sigma}(x)\rho_{r,-\sigma}(x) \right] \tag{4.4}$$

$$H_2 = \int \mathrm{d}x \sum_{\sigma=A,B} \left[g_{p,2}\rho_{R,\sigma}(x)\rho_{L,\sigma}(x) + g_{o,2}\rho_{R,\sigma}(x)\rho_{L,-\sigma}(x) \right] \tag{4.5}$$

$$\tag{4.6}$$

Where (o,p) define if the interaction acts between particles of (different,same) species, and the minus means that we have change species (-A=B, -B=A).
In order to split the Hamiltonian it is convenient to introduce the *total charge* and the *total spin* degrees of freedom defined as

$$\rho_c = \frac{\rho_A + \rho_B}{\sqrt{2}} \quad , \quad \rho_s = \frac{\rho_A - \rho_B}{\sqrt{2}} \tag{4.7}$$

The same unitary transformation can be applied to the boson field and it allows to obtain two new fields (4.8).

$$\phi_c(x) = \frac{\phi_A + \phi_B}{\sqrt{2}} \quad , \quad \phi_s = \frac{\phi_A - \phi_B}{\sqrt{2}} \tag{4.8}$$

There is a similar relation for the field θ.
Using these new fields (4.8), we can re-write the free Hamiltonian as

$$H_0 = H_c + H_s \tag{4.9}$$

$$H_0 = \frac{1}{2\pi} \sum_{i=c,s} \int \mathrm{d}x [(\boldsymbol{\nabla}\phi_i)^2 + (\boldsymbol{\nabla}\theta_i)^2] \tag{4.10}$$

At the same manner we can rewrite the *interacting terms* as

$$H_4 = \frac{1}{4\pi^2} \int \mathrm{d}x [g_{p,4} + g_{o,4}][(\boldsymbol{\nabla}\phi_c)^2 + (\boldsymbol{\nabla}\theta_c)^2] + [g_{p,4} - g_{o,4}][(\boldsymbol{\nabla}\phi_s)^2 + (\boldsymbol{\nabla}\theta_s)^2] \tag{4.11}$$

$$H_2 = \frac{1}{4\pi^2} \int \mathrm{d}x [g_{p,2} + g_{o,2}][(\boldsymbol{\nabla}\phi_c)^2 - (\boldsymbol{\nabla}\theta_c)^2] + [g_{p,2} - g_{o,2}][(\boldsymbol{\nabla}\phi_s)^2 - (\boldsymbol{\nabla}\theta_s)^2] \tag{4.12}$$

In the case of two species we have to consider one more term, that we avoided to use in the spinless fermion case because it was indistinguishable from the others [14].
This is the "g_1" interaction, that is shown in figure 4.1 .

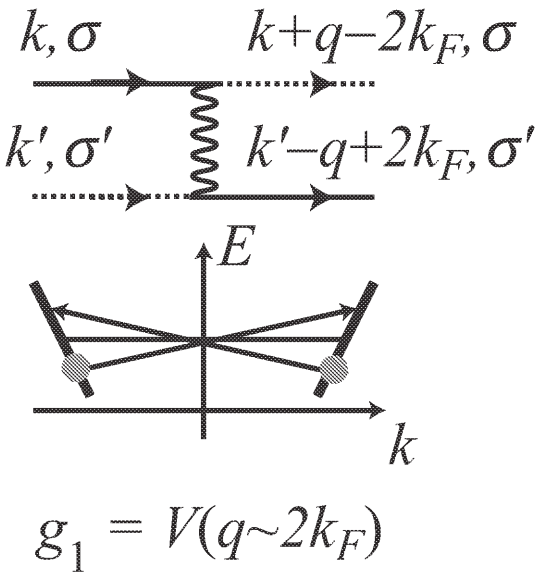

Figure 4.1: Low energy process of interaction, a full line is for a fermion with a momentum close to $+k_F$ (right going fermion) and the dashed line for a fermion with momentum close to $-k_F$(left going fermion).
The σ defines the species (A,B). For fermions of different species the interaction takes the form (g_o,g_p) depending on whether the species σ and σ' are equal (g_p) or opposite (g_o).

Now we can write the Hamiltonian related to the "g_1" interaction, that will take the form

$$\begin{aligned} H_1 &= \int \mathrm{d}x g_{p,1} \sum_\sigma [{c^\dagger}_{L,\sigma} {c^\dagger}_{R,\sigma} c_{L,\sigma} c_{R,\sigma}] + g_{0,1} \sum_\sigma [{c^\dagger}_{L,\sigma} {c^\dagger}_{R,-\sigma} c_{L,-\sigma} c_{R,\sigma}] = \\ &= -\int \mathrm{d}x g_{p,1} \sum_\sigma [{c^\dagger}_{L,\sigma} c_{L,\sigma} {c^\dagger}_{R,\sigma} c_{R,\sigma}] + g_{0,1} \sum_\sigma [{c^\dagger}_{L,\sigma} c_{R,\sigma} {c^\dagger}_{R,-\sigma} c_{L,-\sigma}] = \end{aligned} \tag{4.13}$$

We can see that the first term of (4.13) is the same that for "$g_{p,2}$".
So we can write the $g_{o,1}$ term using the transformations (4.8)

$$\begin{aligned} H_{1,o} &= \int \mathrm{d}x \frac{g_{o,1}}{(2\pi\alpha)^2} \sum_{s=A,B} [e^{i(-2\psi_s(x))} e^{i(2\psi_{-s}(x))}] \\ &= \int \mathrm{d}x \frac{g_{o,1}}{(2\pi\alpha)^2} cos(\sqrt{8}\psi_s(x)) \end{aligned} \tag{4.14}$$

We can rewrite the total Hamiltonian grouping the interaction terms inside new param-

eters (K_σ, u_σ), where $\sigma = c, s$. With some algebra, one gets:

$$H = H_c + H_s$$
$$H_c = \frac{1}{2\pi}\int \mathrm{d}x\,[u_c K_c(\pi\boldsymbol{\nabla}\theta)^2 + \frac{1}{u_c K_c}(\boldsymbol{\nabla}\phi)^2] \tag{4.15}$$
$$H'_s = \frac{1}{2\pi}\int \mathrm{d}x\,[u_s K_s(\pi\boldsymbol{\nabla}\theta)^2 + \frac{1}{u_s K_s}(\boldsymbol{\nabla}\phi)^2] \tag{4.16}$$
$$H_s = H'_s + \int \mathrm{d}x\,\frac{g_{o,1}}{(2\pi\alpha)^2} cos(\sqrt{8}\phi_s(x)) \tag{4.17}$$

Looking at equations (4.15, 4.16) we can see the similarity with the theory of the first chapter (1.26).
We can see that there is a complete separation between the charge and the spin parts.

Observables We have seen that the total Hamiltonian for two species fermions is similar to the spinless fermion Hamiltonian, so we expect that the *density-density correlation functions* have to be quite the same of (1.47).
In fact the *density-density correlation* for two species takes the form (4.18)

$$< \rho(x,0)\rho(0,0) >= {\rho^2}_0 + \frac{K}{\pi^2}\frac{{y^2}_\alpha - x^2}{(x^2 + {y^2}_\alpha)} + {\rho^2}_0 A_2 cos(2\pi\rho_0 x)\left(\frac{\alpha}{x}\right)^{K_s+K_c} + \\ + {\rho^2}_0 A_4 cos(4\pi\rho_0 x)\left(\frac{\alpha}{x}\right)^{K_c} + \dots \tag{4.18}$$

where A_i, α are non universal constants, y_α is the renormalized interaction [14] and ρ_0 is the total density ($\rho_0 = \rho_T$).
It's important to observe that really inside the *spin part* of the Hamiltonian (4.17) there is an additional term linked to the $g_{o,1}$ interaction, it acts changing the power of one of the oscillating terms [14].
Looking at (4.18) we can see that the oscillating term $cos(2\pi\rho_0)$ decays with the power $K_c + K_s$, meanwhile the oscillating term $cos(4\pi\rho_0)$ decays with the power $4K_c$.
From the (4.18) we can extract the *connected part* (4.19)

$${G^{ts}}_2(x) = \frac{K}{\pi^2}\frac{{y^2}_\alpha - x^2}{(x^2 + {y^2}_\alpha)} + {\rho^2}_0 A_2 cos(2\pi\rho_0 x)\left(\frac{\alpha}{x}\right)^{K_s+K_c} + \\ + {\rho^2}_0 A_4 cos(4\pi\rho_0 x)\left(\frac{\alpha}{x}\right)^{K_c} + \dots \tag{4.19}$$

and compute the **structure factor** for the finite lattice as we have seen in the first chapter (1.49):

$$S(k) = \sum_{j,i=1}^{L} e^{ik(j-l)}\frac{{G^{ts}}_2(i-j)}{L} \tag{4.20}$$

where “ts” it means two species.

4.4 Results

Here we start to resume and explain the results obtained from the numerical calculations, giving a theoretical explanation in the framework of the theory introduced before.
We have performed numerical simulations for all the points in the $V - r_c$ plane shown by the black dots in figure 4.2. From now on, we set $t = 1$ and $U = 100$.

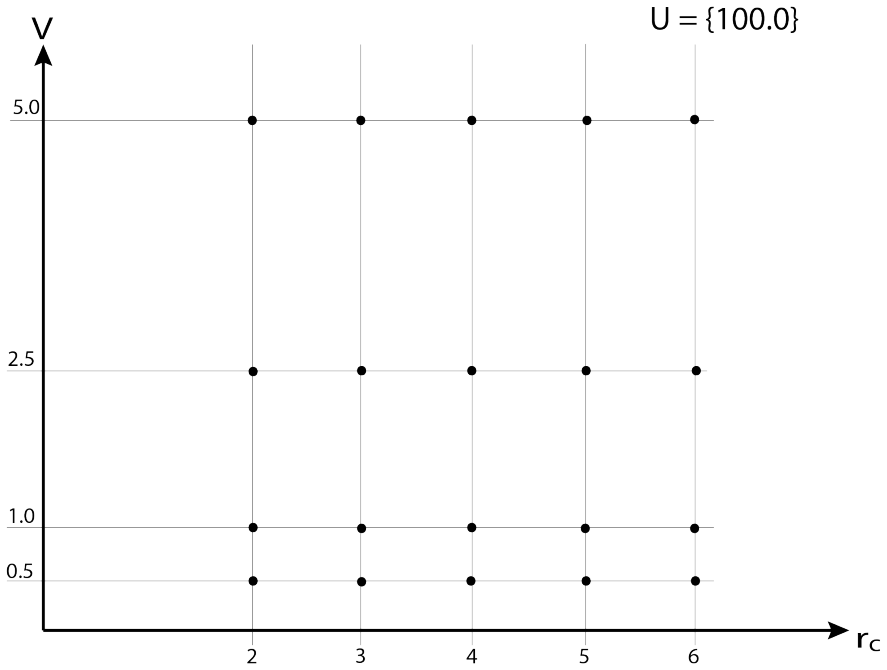

Figure 4.2: Points of the phase diagram explored by numerical calculation for $t = 1$ $U = 100$, $\rho_T = 1/4$, $\rho_A = \rho_B = 1/8$.

For all the calculations we worked with the total lenght fixed (**L=48**), *total density* ($\rho_{\mathbf{T}} = \rho_{\mathbf{A}} + \rho_{\mathbf{B}} = \frac{1}{8} + \frac{1}{8} = \frac{1}{4}$) and a range of the precision between (100, 500) DMRG states.

4.4.1 Structure factor

In this section we will look at the *structure factor* (4.20) plots given by numerical calculation, we focalize on this observable because is well defined in the range of precision on which we worked.

On each graph we will define the number of DMRG states that we considered, we will write them ordered from the lowest to the highest value of the parameter on which they are plotted. We can start to observe the **Structure factor** for $\mathbf{U = 100.0}$ for a lattice of $L = 48$.

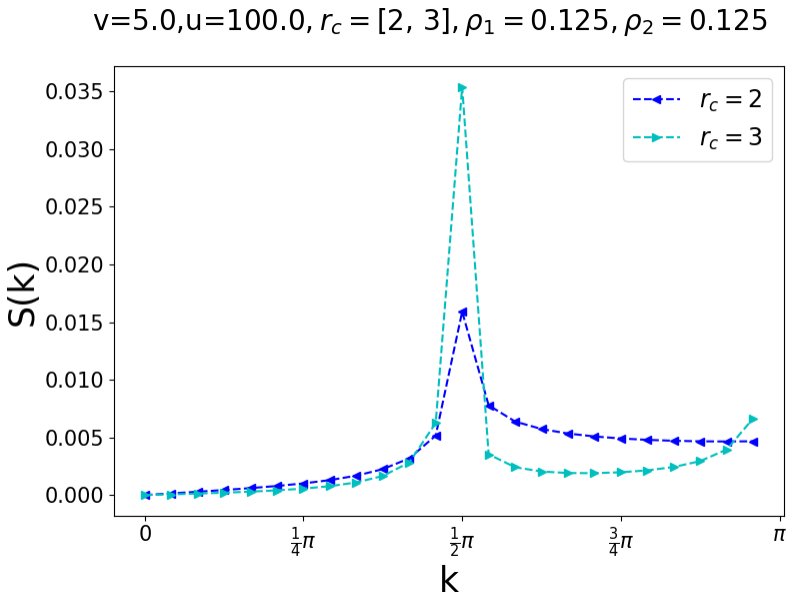

Figure 4.3: Structure factor for $r_c = 2, 3$; $V = 5.0$; $U = 100.0$; $L = 48$. DMRG states 200, 410.

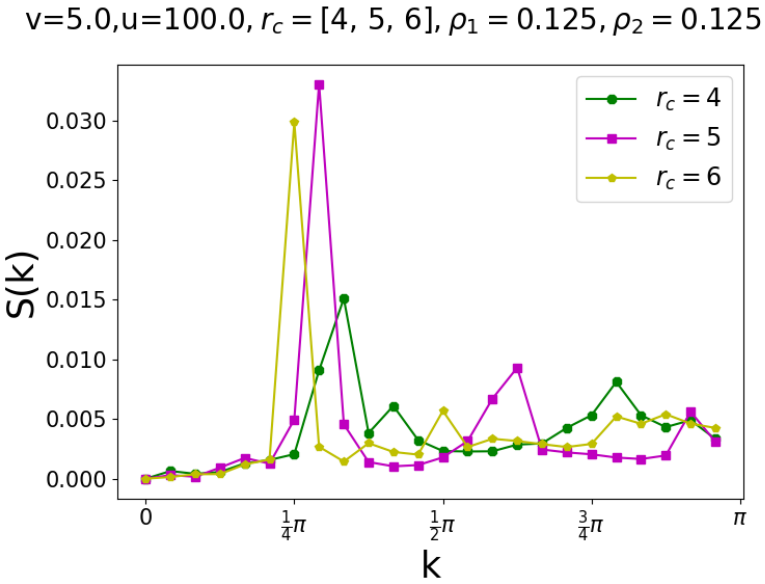

Figure 4.4: Structure factor for $r_c = 4, 5, 6$; $V = 5.0$; $U = 100$; $L = 48$. DMRG states 169, 431, 405.

In figure 4.3 it is analyzed the cases for $r_c = 2, 3$ and $V = 5.0$. We can see that the data are in good agreement with the aforementioned theory. We find that that the peak (k_c) is positioned around $k_c = \pi/2$ as we expect for $\rho_T = 1/4$.
In figure 4.4 it is analyzed the cases for $r_c = 4, 5, 6$ and $V = 5.0$. We can see that is present a shift of the peak.
This change can be explained considering a *cluster count field* (2.13) as it was seen in [27]. This result that comes considering this new field as the change of the argument of the oscillating part of *density-density correlation* function ($2\pi\rho_T x \to 2\pi\rho_T\sigma x$) where the σ is the same of the previous case (2.15).
We can understand that the cluster formation doesn't depend on the species in the *one species limit*, this because the interactions given in the Hamiltonian (4.1) are the same between particles of the same and different species.
From the cluster interpretation we expect the peak of the structure factor at $k_c = 2\pi\frac{1-\rho_T}{r_c}$ that for $r_c = 4, 5, 6$ is $k_c = \pi\frac{3}{8}, \pi\frac{3}{10}, \frac{\pi}{4}$, in very good agreement with the data in figure 4.4.
There is an amazing feature for the case of $r_c = 5$, although the length is not commensurable with the cluster formation we find that the data show the peak of the structure factor where we expect it.
It means that although classically the cluster formation is not possible for commensurability with the lattice, in quantum regime thanks to the superposition of the states the cluster behavior is reached.

Now we can show other peculiar features that are linked to the structure factor.

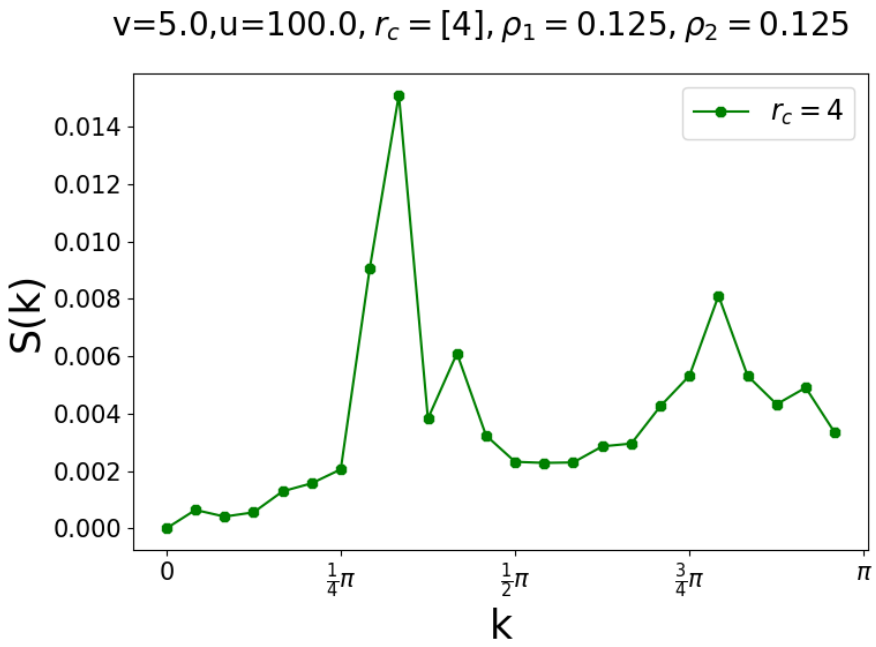

Figure 4.5: Structure factor for $r_c = 4$, $V = 5.0$, $U = 100$, $L = 48$, DMRG states 169.

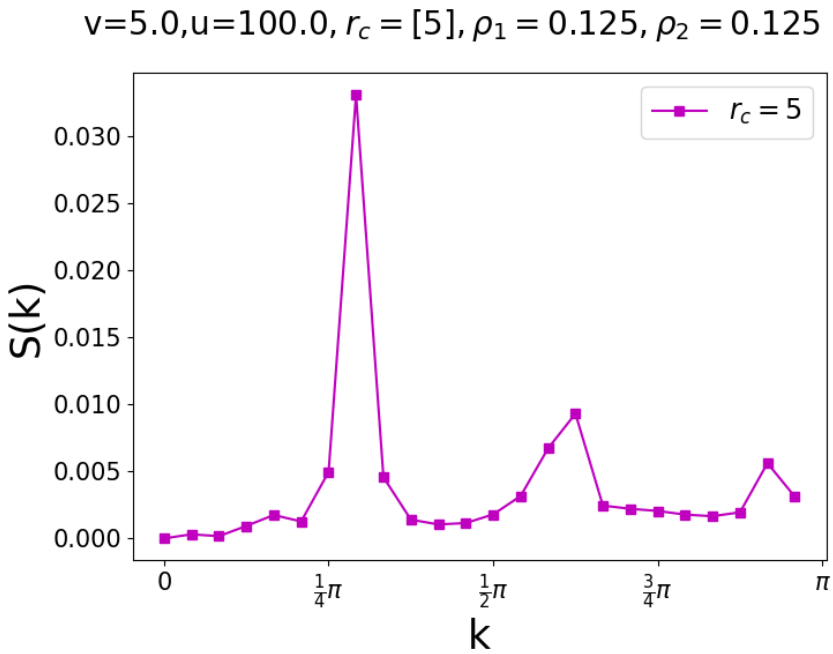

Figure 4.6: Structure factor for $r_c = 5$, $V = 5.0$, $U = 100$, $L = 48$, DMRG states 431.

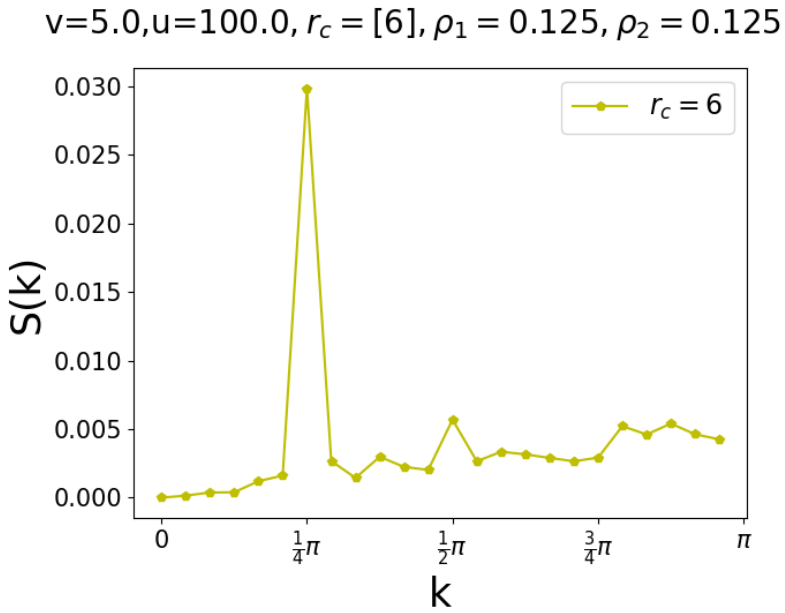

Figure 4.7: Structure factor for $r_c = 6$, $V = 5.0$, $U = 100$, $L = 48$, DMRG states are 405.

For example we can take the graphs 4.5, 4.6, 4.7 to observe some peculiarities inside the structure factor.
In fact we can see there are present some others damped peaks linked to the other oscillating terms present in the (4.18).
We can see that these peaks are localized at $\mathbf{k_c} = 4\pi\frac{1-\rho}{r_c} = \frac{3}{4}\pi, \frac{3}{5}\pi, \frac{1}{2}\pi$ for $r_c = 4, 5, 6$.
Moreover it is possible distinguish a third peak that is not present in our calculation (4.18) but it is present the complete expansion, and it is positioned at $\mathbf{k_c} = 6\pi\frac{1-\rho}{r_c} = \pi, \frac{9}{10}\pi, \frac{3}{4}\pi$ for $r_c = 5, 6$.
These features show the strong agreement between data and the underlying theory.
Another important question is to find the boundaries of the phases by observing the trend of the structure factor varying the value of coupling.

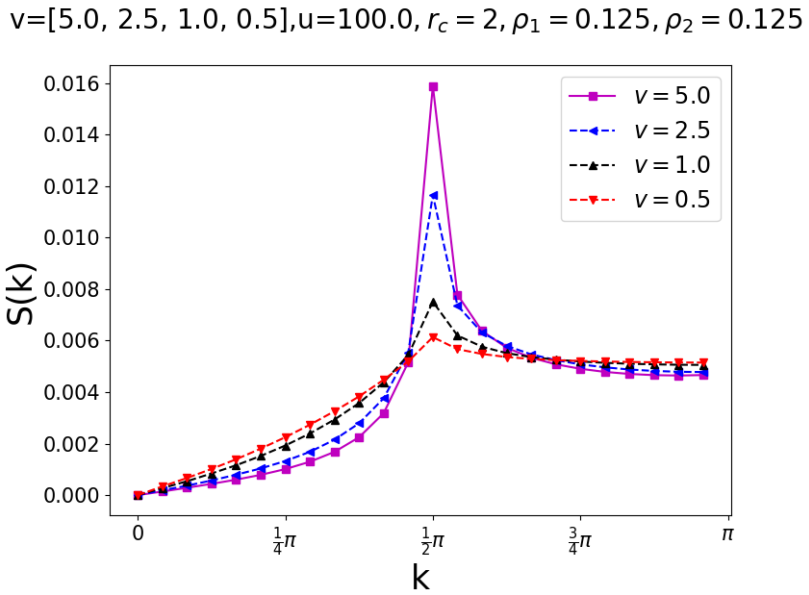

Figure 4.8: structure factor for several V, $r_c = 2$,$U = 100$, $L = 48$, DMRG states 102, 108, 152, 200.

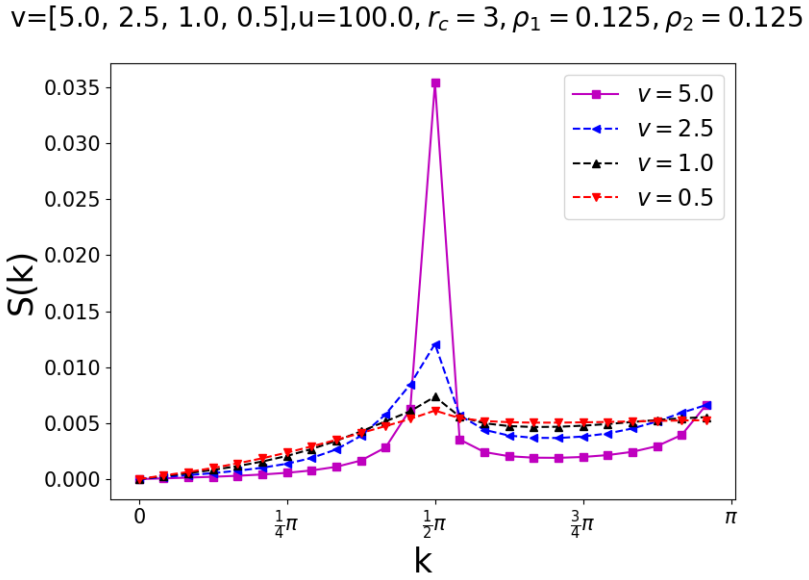

Figure 4.9: structure factor for several V, $r_c = 3$, $U = 100$, $L = 48$, DMRG states 260, 205, 405, 410.

From the graphs shown in figures 4.8, 4.9 we can see that decreasing the strength

of the coupling (V), the peak of the structure factor decreases. For for $V = 0.5$ the structure factor seems the same for both.

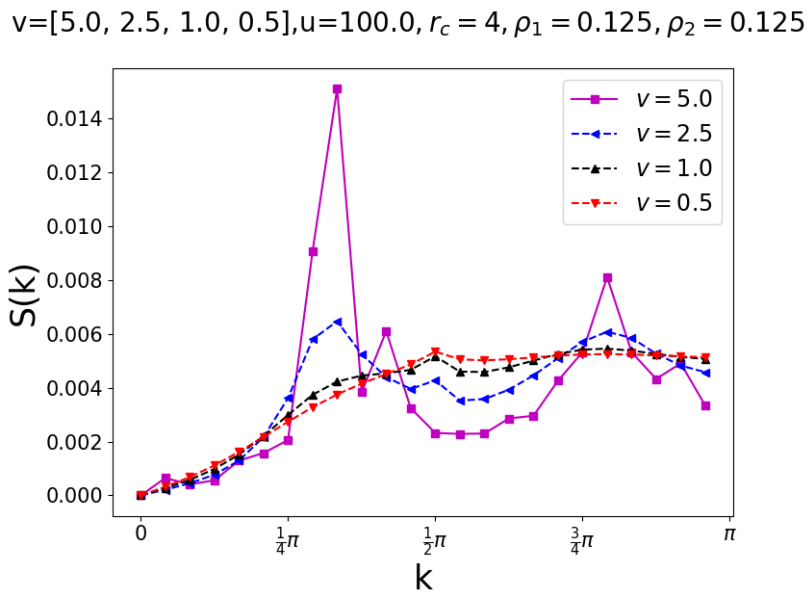

Figure 4.10: Structure factor for several V, $r_c = 4$, $U = 100$, $L = 48$, DMRG states 200, 200, 200,169.

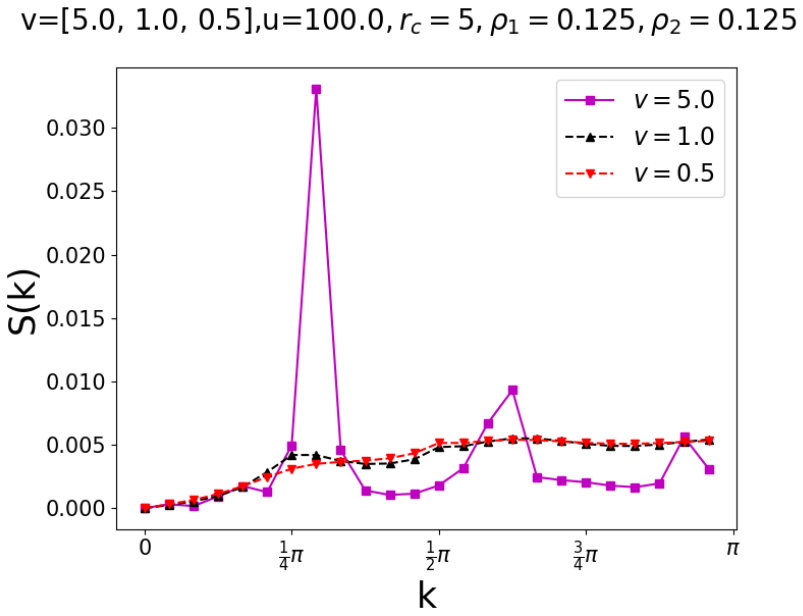

Figure 4.11: Structure factor for several V, $r_c = 5$, $U = 100$, $L = 48$, DMRG states 413, 424, 413.

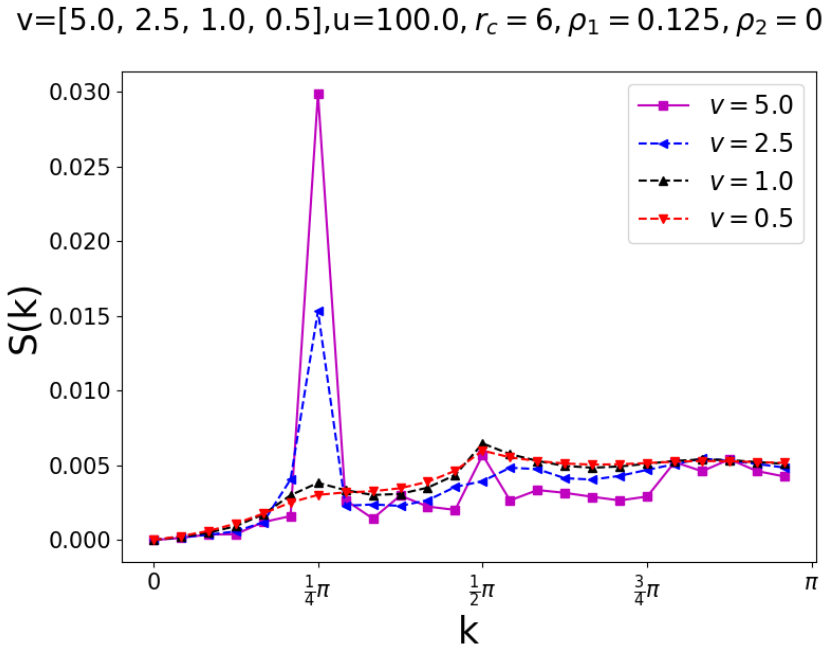

Figure 4.12: Structure factor for several V, $r_c = 6$, $U = 100$, $L = 48$, DMRG states 405, 403, 440, 413.

Looking at the graphs shown in figures 4.10, 4.11, 4.12 we can see that decreasing the strength of the coupling the peak of the structure factor decreases, and for $V = 0.5$ the graphs seem to be similar to the case of $r_c = 2, 3$ for the same coupling.
From all the graphs is possible to see that there is a transition below a certain value of the interaction (V=0.5) where all the plots of the structure factor take the same form.

We can summarize saying that for $r_c = 2$ we find the Luttinger liquid behavior for all the strengths of coupling.
For $r_c = 3$ the structure factor seems consistent with the crystal phase and we can notice that between the peaks at $V = 2.5$ and $V = 5.0$ there is a big distance, so we can imagine there takes place a phase transition between crystal and LL as suggested by the one-species case [27].
For $r_c = 4, 5, 6$ we can see that the cluster paradigm still holds until $V = 0.5$.
Under this threshold it is possible to observe a phase transition between CLL and LL, this transition can be explained saying that below $V = 1$ the hopping part starts to dominate , so the system always behaves like a Luttinger liquid.

Conclusion

In summary, looking at the phase diagram of the *extended Hubbard model with soft-shoulder interaction* in the *one-specie limit*, explained in the last chapter, we can see that it presents three different phases: Luttinger liquid, crystal, cluster Luttinger liquid. This is in great agreement with the theory.
We can see that this behavior is quite the same observed for the case of spinless fermion systems with soft-shoulder interaction [27]. Moreover it is possible to observe that both the models present the same phase transitions between LL and CLL and between crystal and LL.
This fact can be explained considering that if we work in this limit, where the (U) interaction are energetically avoided, the other (V) interaction, as we implemented, doesn't distinguish between the species. This leads to expect an identical behavior between them, as we found until now.
This analysis is just the starting point of an interesting and deep analysis that has to be done to well understand the features of the complete phase diagram of the model.

Bibliography

[1] A. Auerbach, *Interacting electrons and quantum magnetism*, Graduate Texts in Contemporary Physics (Springer New York, 1998).

[2] A. Balachandran, E. Ercolessi, G. Morandi, and A. Srivastava, *The hubbard model and anyon superconductivity*, (World Scientific) Lecture Notes in Physics (1990).

[3] S. Banerjee, and A. Roy, *Linear algebra and matrix analysis for statistics*, Chapman & Hall/CRC Texts in Statistical Science (Taylor & Francis, 2014).

[4] I. Bloch, J. Dalibard, and W. Zwerger, "Many-body physics with ultracold gases", Rev. Mod. Phys. **80**, 885–964 (2008).

[5] P. Calabrese, and J. Cardy, "Entanglement entropy and quantum field theory", JSTAT **2004**, P06002 (2004).

[6] P. Calabrese, and J. Cardy, "Entanglement entropy and conformal field theory", J. PHYS. A-MATH. THEOR. **42**, 504005 (2009).

[7] J. L. Cardy, and I. Peschel, "Finite-size dependence of the free energy in two-dimensional critical systems", Nucl. Phys. B **300**, 377–392 (1988).

[8] M. A. Cazalilla, "Bosonizing one-dimensional cold atomic gases", J. Phys.B **37**, S1–S47 (2004).

[9] C. Cohen-Tannoudji, B. Diu, and F. Laloë, *Quantum mechanics, volume 1-2*, Trans. of : Mécanique quantique. Paris : Hermann, 1973 - (Wiley, 1977).

[10] M. Dalmonte, W. Lechner, Z. Cai, M. Mattioli, A. M. Läuchli, and G. Pupillo, "Cluster luttinger liquids and emergent supersymmetric conformal critical points in the one-dimensional soft-shoulder hubbard model", Phys. Rev. B **92**, 045106 (2015).

[11] C. Degli Esposti Boschi, E. Ercolessi, F. Ortolani, and M. Roncaglia, "On c = 1 critical phases in anisotropic spin-1 chains", EPJ B **35**, 465–473 (2003).

[12] P. Di Francesco, P. Mathieu, and D. Sénéchal, *Conformal field theory*, Graduate Texts in Contemporary Physics (Springer, 1997).

[13] T. F. Gallagher, *Rydberg atoms*, Cambridge Monographs on Atomic, Molecular and Chemical Physics (Cambridge University Press, 1994).

[14] T. Giamarchi, *Quantum physics in one dimension*, Internat. Ser. Mono. Phys. (Clarendon Press, 2004).

[15] P. H. Ginsparg, "APPLIED CONFORMAL FIELD THEORY", in Les houches summer school in theoretical physics: fields, strings, critical phenomena les houches, france, june 28-august 5, 1988 (1988), pp. 1–168.

[16] S. Giorgini, L. P. Pitaevskii, and S. Stringari, "Theory of ultracold atomic fermi gases", Rev. Mod. Phys. **80**, 1215–1274 (2008).

[17] N. Goldman, J. C. Budich, and P. Zoller, "Topological quantum matter with ultracold gases in optical lattices", NAT. PHYS. **12**, 639–645 (2016).

[18] M. Henkel, *Conformal invariance and critical phenomena*, Texts and monographs in physics (Springer, 1999).

[19] N. Henkel, R. Nath, and T. Pohl, "Three-Dimensional Roton Excitations and Supersolid Formation in Rydberg-Excited Bose-Einstein Condensates", Phys. Rev. Lett. **104**, 195302, 195302 (2010).

[20] E. Jeckelmann, "Density-matrix renormalization group methods for momentum- and frequency-resolved dynamical correlation functions", PROG. THEOR. PHYS. SUPP. **176**, 143–164 (2008).

[21] N. Kavakami, and S. Yang, "Conformal field theory approach to one dimensional quantum liquids", Progress of Theoretical Physics Supplement (1992).

[22] N. Kawakami, and S.-K. Yang, "Conformal field theory approach to one-dimensional quantum liquids", PROG. THEOR. PHYS. SUPP. **107**, 59 (1992).

[23] L. Komzsik, *The lanczos method: evolution and application*, Software, Environments and Tools (Society for Industrial and Applied Mathematics, 2003).

[24] L. Landau, E. Lifshitz, and L. Pitaevskij, *Statistical physics part 2, theory of condensed state*, Landau and Lifshitz Course of theoretical physics (Oxford, 1980).

[25] J. Lim, H.-g. Lee, and J. Ahn, "Review of cold rydberg atoms and their applications", JKPS **63**, 867–876 (2013).

[26] E. Y. Loh, J. E. Gubernatis, R. T. Scalettar, S. R. White, D. J. Scalapino, and R. L. Sugar, "Sign problem in the numerical simulation of many-electron systems", Phys. Rev. B **41**, 9301–9307 (1990).

[27] M. Mattioli, M. Dalmonte, W. Lechner, and G. Pupillo, "Cluster luttinger liquids of rydberg-dressed atoms in optical lattices", Phys. Rev. Lett. **111**, 165302 (2013).

[28] G. Mussardo, *Statistical field theory: an introduction to exactly solved models in statistical physics*, Oxford Graduate Texts (OUP Oxford, 2010).

[29] M. A. Nielsen, and I. L. Chuang, *Quantum computation and quantum information: 10th anniversary edition*, 10th (Cambridge University Press, 2011).

[30] P. Nozieres, and D. Pines, *Theory of quantum liquids*, Advanced Books Classics (Avalon Publishing, 1999).

[31] I. Peschel, *Density matrix renormalization: a new numerical method in physics*, Lecture notes in physics (Springer Verlag, 1999).

[32] D. Petz, *Quantum information theory and quantum statistics*, Theoretical and Mathematical Physics (Springer, 2008).

[33] S. Rao, and D. Sen, "An introduction to bosonization and some of its applications", arXiv preprint cond-mat/0005492 (2001).

[34] U. Schollwöck, "The density-matrix renormalization group", Rev. Mod. Phys. **77**, 259–315 (2005).

[35] U. Schollwöck, "The density-matrix renormalization group in the age of matrix product states", Annals of Physics **326**, 96–192 (2011).

[36] U. Schollwock, "The density-matrix renormalization group: A short introduction", Phil. Trans. Roy. Soc. Lond. **A369**, 2643–2661 (2011).

[37] G. L. G. Sleijpen, and H. A. V. der Vorst, "A jacobi–davidson iteration method for linear eigenvalue problems", SIAM J. MATRIX. ANAL. A **17**, 401–425 (1996).

[38] J. Voit, "A brief introduction to Luttinger liquids", in American institute of physics conference series, Vol. 544, American Institute of Physics Conference Series (Nov. 2000), pp. 309–318.

Acknowledgements

I would like to express my sincere gratitude to my advisor Prof. Elisa Ercolessi for her patience, support, availability, and mostly for the knowledge she shared with me and all the passion she conveyed me.
I'm very thankful to Prof. Guido Pupillo, that introduced me to the study of a very interesting research topic. Besides, I'm grateful to him because he gave me the chance to pass three months working in direct contact with his team, and understanding the real meaning of research, in Strasbourg.// A special thanks go to Prof Fabio Ortolani that gave me many indispensable advices to understand how to work in numerics.
I'm very thankful to Adriano, Fabio, Thomas, the researchers at the Université de Strasbourg, for the many advices they gave me.
I'm very thankful to my friends and colleagues Luca, Enrico, Paolo for the long discussions about physics.
A sincerely thanks go to Filippo Ravaglia that really helped me to understand the secrets of Python.
But the best thanks go to Silvia for her constant support and for giving me the force to follow my passions.
Words cannot express my gratitude for my family that gave me the opportunity to cultivate my passion for physics.